NASA Contractor Report 165300

THERMAL FATIGUE BEHAVIOR OF H-13 DIE STEEL FOR ALUMINUM DIE CASTING WITH VARIOUS ION SPUTTERED COATINGS

C. Y. Nieh and J. F. Wallace

Case Western Reserve University
Cleveland, Ohio

July 1981

Prepared for

NATIONAL AERONAUTICS AND SPACE ADMINISTRATION
Lewis Research Center
Under Grant NSG-3279

CONTENTS

THERMAL FATIGUE BEHAVIOR OF H-13 DIE STEEL FOR ALUMINUM DIE CASTING WITH VARIOUS ION SPUTTERED COATINGS

C. Y. Nieh* and J. F. Wallace**

Case Western Reserve University
Cleveland, Ohio

SUMMARY

This investigation was conducted to determine the effect of various ion-deposited coatings on the thermal fatigue resistance of H-13 die steels for aluminum-die-casting dies. Various coatings were applied to a special 2-inch-square, 7-inch-long thermal fatigue test specimen by the ion sputter deposit method. The thermal fatigue specimen was internally water cooled and alternately immersed in molten aluminum and cooled in air. After 15 000 cycles the thermal fatigue cracks at the specimen corners were measured. The types of coatings studied were Mo, W, Pt, Ag, Au, Co, Cr, Ni, Ag + Cu, Mo + Pt, W + Pt, Si_3N_4, AlN, Cr_3C_2, Ta_5Si_3, and ZrO_2.

The results of the thermal fatigue tests on the coated specimens indicated that a significant improvement in thermal fatigue resistance was obtained with platinum, molybednum, and tungsten coatings. The other types of coatings either did not affect the thermal fatigue resistance to any significant degree or lowered the resistance. Metallographic examination of the coatings indicates that the improvement in thermal fatigue resistance resulted from protection of the surface of the die steel from oxidation. The oxide entered any cracks formed at corrosion pits or other discontinuities and caused cracks to propagate by producing a tensile stress from the volume increase of the oxide at the crack tip. The high yield strength and ductility of molybdenum and tungsten contributed to the better thermal fatigue resistance.

INTRODUCTION

Dye casting[1-3] refers to a casting process in which liquid metal is introduced into a die under relatively high pressure and held against the die wall until solidification occurs. The process is widely used today for the high-speed, high-quantity production of fairly intricate parts from nonferrous metals.[4,5] The close dimensional tolerance, good detail, and smooth surface finish of the die castings minimize the number of finish operations required. Thermal fatigue damage to the die reduces the quality of the die-casting surface. Eventually the cracks produced become so severe that the die has to be replaced or discarded.

The dies employed in die casting are relatively expensive, so their life or durability is a major economic consideration of the die-casting process. Depending on the intricacy and complexity of the die, the cost of a die may be more than the heavy machine required to operate it. Dies for aluminum alloys cost approximately 50 percent more than those for the lower-melting-temperature alloys because the higher strength alloy die steel

---

*Graduate Student.

**Republic Steel Professor and Chairman of the Department of Metallurgy and Materials Science.

required is more costly. Therefore increasing the number of castings that can be produced in a die is of even greater importance in aluminum die casting.

The principal failure modes of aluminum-die-casting dies are considered to be heat checking or thermal fatigue; corrosion or corrosion fatigue; gross cracking; and erosion of the die surface. Heat checking occurs by the development of fine cracks in the surface that frequently form a cross-hatched pattern. These cracks increase in length and depth with the number of castings. They leave a corresponding network of fins on the die casting. When these fins can no longer be removed economically or when they interfere with the operation, the die must be removed from production for repair or replacement.

Both the initiation and propagation of thermal fatigue cracks involve corrosion. The surface of a die in service is covered by an oxide layer. As a result of this oxidation, corrosion pits are produced in the casting surface and are filled with oxides. Since the oxides occupy a larger volume than the metal that they replace, this exerts a wedging effect and tensile stresses at the crack tip. These stresses propagate the thermal fatigue cracks into the die.

Gross cracking is not generally as prevalent as heat checking and corrosion. When it does occur, it is severe and can result in complete cracking through the die.[6] Gross cracking is produced by relatively large stresses on the die, usually of a thermal nature. These cracks are more prone to occur at lower temperatures than heat checking or in die steels of lower fracture toughness.[6,7] They may initiate from the deeper heat checks.

Erosion usually occurs around the gate location where the high-temperature and high-pressure molten metal stream is injected into the die cavity. Characteristically the steel appears to be washed away.[8,9] This type of failure occurs by physically wearing the die steel by mechanical action as well as by its solution in the molten die-casting alloy.[10] An eroded die must be discarded or repaired when the cavity or gating has enlarged so that the weight, castability, or dimensional stability of the casting are affected sufficiently that the casting is unusable.

Thermal stresses occur in the die steel from temperature gradients developed within the die cross section by heating and cooling at the die surface. The temperature changes produce thermal stresses when the thermal expansion or contraction of a section is restrained by its surroundings. In the simple case of a bar with fixed end supports, the thermal stress developed[11,12] by a temperature change ΔT is

$$\sigma = \alpha E \Delta T$$

where α = linear thermal coefficient of expansion
E = elastic modulus

A thermal fatigue specimen used in the present investigation is shown in figure 1. These tests were employed because they were capable of producing the desired amounts of constraint and thermal fluctuation at the corners of the square. A predominately uniaxial stress condition occurred at the edges during thermal fatigue cycling, and the thermal fatigue cracks were primarily produced at the edges or corners of the specimen. The stress state at the edge was similar to that of the prism-shaped specimen used for

thermal fatigue tests by Northcott,[13] where a one-dimensional stress developed along the edge. When the temperature variation ΔT developed in these tests is sufficiently high, the surface layer can be plastically deformed in compression at the surface. During cooling the surface may contract sufficiently to relieve the induced compression stress and produce a residual tensile stress because it has been shortened by the plastic compression. This residual stress pattern was observed in the present test. Graham[14] observed, during cutting of a 3/8-inch-square by 7-inch-long coupon from the corner of a thermal fatigue specimen such as that shown in figure 1 that each 3/8-inch-square strip bowed inward slightly when cut off the specimen. It is generally considered that a tensile stress on the surface of the die is required to initiate a crack. Graham[14] used the finite element method to investigate the temperature gradient and stress distribution in the cross section of the test specimen, with the results shown in figures 2 and 3. The cycle compressive stress shown in figure 3 was computed at the corner of the thermal fatigue specimen shown in figure 1. The yield strength of the H-13 die steels used is about 120 ksi at 1100° F; this strength is higher than the maximum compressive stress (75 ksi) calculated by Grahm. However, the results do indicate some upsetting of the corner. This could result from some localized flaw under the alternating compression stresses; from tempering and softening of the steel sufficient to lower its yield strength; or from the additional compressive stress at the corner produced by the larger volume of the oxidized metal within the cracks. Softening of the die steel around the surface was observed in a microhardness study conducted by Graham after testing for 15 000 cycles. It is noted that thermal fatigue is primarily responsible for eventual failure not only of die-casting dies but of other components subjected to fluctuating thermal cycles such as hot rolls, forging tools, dies, and ingot molds.[15-18]

In the die-casting process when the molten metal is injected into a mold or die cavity, the surface of the die is immediately subjected to a severe temperature rise. This temperature is rapidly decreased by conduction of heat into the underlying die metal. The magnitude of this temperature fluctuation is determined by the heat transfer characteristics at the surface because of coatings, oxide layers, and dimensional configurations. The combination of cyclic thermal stressing and environmental effect causes the heat checking on die-casting dies.

Corrosion fatigue[19-21] is defined as the reduction of fatigue resistance caused by the presence of a corrosive environment in addition to an alternating stress. The fatigue cracks subject to corrosion contain corrosion products although the presence of these products does not necessarily indicate corrosion fatigue. In the die-casting process the surface of the die is subjected to an aggressive environment of high temperature, steam, lubricant spraying, and liquid metal. A black or dark brown surface film is always present on a working die and consists of the degradation product of the lubricant together with metallic oxides from the die. Corrosion pits are also generally present in the die surface and act as stress raisers for fatigue crack initiation. Accordingly, conditions for corrosion fatigue are present; the thermal cycles provide alternating stress and the oxidizing conditions furnish the corrosive environment. This combination of conditions provides the oxide-filled, transgranular cracks that follow a path perpendicular to the maximum uniaxial stress. The thickness of the oxide decreases at greater depths into the cracks.[22] This

corrosion fatigue of the die resulting from the oxidizing conditions and alternating stresses has been described by other investigators.[5,23-25]

Corrosion fatigue can be reduced by lowering the stress on the components, and it is possible that a stress-relieving heat treatment may be beneficial. This corrosion fatigue can also be minimized by improving the corrosion resistance of the die by applying a coating that prevents die metal contact with an oxidizing environment. The coating techniques should neither produce a tensile stress in the coating nor charge hydrogen into the metal. Coatings deposited by ion beam sputtering appear to offer possibilities of providing such desirable protection to the die surface.

Ion beam technology has been developed for spacecraft use because of the recent efforts on ion thruster systems for flight applications. This mature technology is transferable to a wide range of nonpropulsive applications.[26] One of the generic industrial applications of this ion propulsive technique is ion beam sputtering deposition.

Argon or xenon can be used for the ion source. The gases are ionized inside the discharge chamber shown in figure 4. The ions are accelerated by a dished-grid beam extraction system and form a stable ion beam. The bombardment of the ionized gas causes the target to slowly disintegrate. The disintegrated materials may be deposited in one of two ways: (1) as free atoms or aggregates or (2) in chemical combination with the controlled atmosphere. The latter of these two methods is employed for the depositon of oxides and nitrides.

One advantage of the sputtering method is the comparatively easy deposition of high-melting-point refractory metals such as tungsten, molybdenum, and tantalum. Another advantage is that an alloy can be deposited with only slight, if any, fractional distillation. The deposited coatings are uniform in thickness and adhere tightly to the substrate. The disadvantage of ion beam sputtering is the slow deposition rate; minutes and sometimes hours are often required for the deposition of a coating only 1000 angstroms thick.

This investigation was undertaken to determine whether selected ion-sputtered coatings on H-13 die steel would have the potential of improving the thermal fatigue behavior of the steel for use as a die in aluminum die casting. The coatings were selected to test materials that included insulators and metals capable of providing protection of the die surface from oxidation.

MATERIALS AND PROCEDURE

The thermal fatigue specimens tested in this investigation were machined from 2.5-inch-square or 3-inch-diameter-round bars designated S (for square) and R (for round). The bars were machined to the dimensions shown in figure 1 with a 0.050-inch allowance for grinding after heat treatment. The chemical composition and heat numbers of the steels are given in table I.

A 1/2-inch-thick test piece was also cut from each bar and sectioned into four small pieces to monitor the hardness and microstructure during the heat treatment. These small pieces were inserted into the interior of the specimens during heat treatment. All specimens were austenitized at 1850° F for 2 hours and then oil quenched and step tempered to about a 46 Rockwell C hardness. Table II shows the hardness and the heat-treating procedure.

After tempering, the exterior surface of each specimen was surface ground to the final dimensions shown in figure 1 to remove any decarburized

layer. The corners of each specimen were then hand ground to a radius of 0.010 inch since this radius dimension in critical. The corners were initially ground with 240 grit paper, clamped on a V-shaped fixture, and finished with 400 grit paper in this same fixture. All radii were checked with a radius gage.

Three corners of the thermal fatigue specimens were coated with different materials by the ion beam sputter deposition method; one corner was left without a coating as a control. The coatings were applied under the direction of Dr. Michael J. Mirtich of the NASA Lewis Research Center. Many details of the coating process and coating adherence are described in an NASA report.[27] An argon ion beam source is used for both the sputter cleaning and sputter deposition. Prior to the insertion of the specimen into the vacuum facility, the specimens were subjected to cleanings in 2 percent NA500 and Linquinex soap solution, followed by rinsing in distilled water and drying with nitrogen. This procedure was followed three times. Before deposition the target (coating material) and substrate (specimen) were sputter cleaned by putting them under the ion beam for 1/2 hour at a beam energy of 1000 electron volts and a current density of 2 mA/cm^2. During the deposition the specimen was wrapped by a metal jacket to protect those areas not to be coated. The specimen was mounted on a push-pull rod that could be retracted through a vacuum chamber gate valve, as illustrated in figure 5. The specimen was 19 centimeters from, and normal to, the target; the target was at 45° with respect to the incident ion beam. The relative positions of ion beam source, target, and substrate are shown schematically in figure 6. The actual apparatus is illustrated in figure 7, and the finished specimen with coatings of cobalt, gold, and tungsten shown counterclockwise is depicted in figure 8. The ion-beam-deposited coatings that were tested for their thermal fatigue behavior are listed in table III.

A schematic illustration of the thermal fatigue testing apparatus is shown in figure 9. The testing procedure has been described in detail by previous investigators.[6,7,28-30] In brief, it consists of alternately cycling the specimen in ambient air and molten 380 aluminum alloy maintained in the crucible furnace at 1300° F. Two Chromel-Alumel thermocouples are used for automatic control and recording of the temperature. The cooling water continuously flows through the specimen at a rate of 1.0 gallon per minute. The cycle includes 13 seconds heating by immersing the specimen into the molten aluminum alloy bath and 23 seconds cooling after removal from the molten metal. The combination of the internal cooling water, surrounding air, and lubricant spray cools the specimen rapidly. Immediately prior to immersion of the specimen, a water-soluble die lubricant (Chem Trend F-3-L) diluted to 50 to 1 by water is sprayed automatically on the surface of the specimen. These die lubricants are widely used in the die-casting process.[31,32] Their application reduces the die temperature at the point of application; this can increase thermal stress and promote heat checking.[33] Therefore the level of lubricant has to be carefully adjusted during the test. To insure the uniform application of the lubricant, the test specimen was turned 90° along the long axis of the specimen every 3750 cycles. This test provides a combination of molten metal heating, water cooling, and lubricant spraying to simulate the conditions prevalent in the aluminum-die-casting process. The influence of erosion from the high velocity of the molten aluminum alloy and the pressure against the die was not simulated by this test.

The specimen was removed from the test apparatus after 15 000 cycles, and the surface oxide layer was removed by the shaped block fixture and 240

grit and 400 grit papers. Cracks within the central 3 inches of each of the four edges were measured at a magnification of 200 in a Leitz microhardness unit.

Two parameters were used to characterize the degree of thermal fatigue cracking. The largest crack on each edge was recorded and is referred to as "the maximum crack length." The term, Σnd^2, is referred to as "the cracked area." The length of each crack was multiplied by the number of cracks n within that crack length group. These nd^2 terms are then added to provide a Σnd^2 value for each edge.

Metallographic specimens were prepared from selected corners of specimens within the central 3-inch length. These specimens were examined by optical microscopes to investigate the shape and path of the thermal fatigue cracks. The relationship between the coating, the oxide layer, and the matrix structure was also studied. The specimens used for metallographic examination were ground on only one side of each corner so that the oxide layer and the coating could be examined on the other untouched side. A 3/8-square-inch bar was cut from each corner of the specimen. The central 3-inch portion of this 3/8-square-inch bar was sectioned transversely into several small pieces about 3/8 cubic inch each. The transverse view of the coating, the oxide, and the base metal was examined by providing a metallographic polish on this surface. Some small pieces were also cut diagonally from the edge toward the center of the specimen, with the plane of polish parallel to the long axis of the specimen. These specimens were examined after polishing to observe the oxide layer, the coating, and the crack behavior. Cracks on the surface of the specimen were examined after step grinding through the oxide layer.

The fractured surface of the thermal fatigue crack was investigated in the scanning electron microscope. Cracks through the 3/8-inch bar were fractured through existing cracks and the exposed surfaces examined by the scanning electron microscope (SEM). The diagonally and transversely cut, polished specimens were also examined by the SEM after etching with 4 percent nital.

Energy dispersive analysis of X-rays (EDAX) was employed, qualitatively or semi-quantitatively, to determine the changes in chemical composition near the surface and the surrounding cracks. The oxides observed on the surface of the fractured cracks appear to be similar to those observed in the polished specimens. In both instances the metal surface at the cracks was completely covered with oxides. The various constituents present in these cracks and on the surfaces were identified by EDAX analysis.

The thermal fatigue specimems included a control specimen that had no ion-sputtered coatings. The testing of this specimen resulted in considerable scatter in the thermal fatigue behavior from one corner to another. This scatter was removed by rotating the specimen 90° every 3750 cycles as previously mentioned to equalize this result. This equalization was rechecked on an extra test from reference 7, and it was determined that the differences in thermal fatigue behavior between corners were eliminated by this rotation.

RESULTS AND DISCUSSION

Thermal Fatigue Behavior

The results of the thermal fatigue tests are listed in table III; the maximum crack lengths and the cracked areas Σnd^2 are plotted as bar

graphs in figures 10 and 11, respectively. For each specimen the results for the various coatings and the control are presented in the order of decreasing thermal fatigue resistance. Each specimen has one control corner without any coating that is used to provide relativity between the different specimens. Because some difficulty was experienced with lubricant control, the two specimens plotted last were tested under more severe conditions.

Some coatings such as gold (Au), cobalt (Co), silicon nitride (Si_3N_4), chromium (Cr), nickel (Ni), copper plus silver (Cu + Ag), and zirconia (ZrO_2) exerted very little effect on thermal fatigue resistance. When these coatings were present, the maximum crack length and the cracked area were similar on both the coated corners and the control corner. Coatings of tantalum silicate (Ta_5Si_3) and silver (Ag) provided poorer thermal fatigue resistance than was obtained on the control corners. Three ion-deposited coatings, tungsten (W), molybdenum (Mo), and platinum (Pt), distinctly improved thermal fatigue resistance. The molybdenum and platinum coatings lowered both the maximum crack length and cracked area values. The tungsten-coated specimen also exhibited a reduced cracked area, but in some cases the maximum crack lengths are comparable to that for the control corner.

One specimen was tested as a control with no coating on any of the four corners. This specimen, which was run during the early stages of the project, showed considerable scatter of thermal fatigue behavior among the corners. Based on these results the procedure of rotating the specimen 90° after every 3750 cycles was introduced into subsequent tests to balance any variation in lubricant spraying from corner to corner. Because one corner of this specimen (S1) was ground to too large a radius (~0.030 in.), it did not crack to any large extent and so the results were discarded. For the same reason the results of one corner of specimen R2 were also discarded. As noted previously specimens R7 and R5 had been subjected to larger amounts of lubrication, producing greater amounts of thermal fatigue cracking at both the control corner and the coated corners. With this increased amount of lubrication, the 0.5-micrometer-thick tungsten coating no longer had good resistance, although 1.0- and 2.0-micrometer-thick coatings still exhibited good thermal fatigue resistance.

One of the important requirements of coatings in order to be effective is adherence to the substrate. Without sufficient bond to the die surface the coating is subjected to failure from many sources such as mechanical loading, thermal stressing, and differential expansion. In this case the coating materials deposited by the ion beam sputter deposition method on the corners of the thermal fatigue specimen had excellent adherence to the die steel.[27]

In addition to adherence the coating has to remain intact on the die steel surface to be effective in inhibiting the corrosive effect of oxidation. When the coating fractures, oxidation can occur directly on the die steel. None of the coatings tested did remain completely intact for the 15 000 cycles. However, coatings such as molybdenum and tungsten do last a significant length of time and improve the thermal fatigue resistance, at least until the coating is fractured. In effect, the coatings inhibit oxidation and suppress crack initiation as long as they are intact. Once the coating has broken down, it apparently may cause more rapid crack propagation at the fractured sites by concentrating both the thermal stress and oxidation at these locations.

Metallographic Examination Results

Only the platinum, molybdenum, and tungsten coatings, which exhibited better results after the thermal fatigue test, were examined metallographically. The control corner, without a deposited coating, was also examined as a comparison with the coated corners. Figure 12 demonstrates the role of oxides in thermal fatigue cracking of control corners. This specimen had its plane of polish in a diagonal of the thermal fatigue test specimen, parallel to the long axis of the specimen. An oxide-lubricant layer covered the surface and oxide filled the cracks propagating into the steel. Figure 13, which provides a transverse view of the control corner, shows that the lubricant oxide layer covered the surface of the control corner. The area close to the oxide appears to be more reactive to the etching solution. Microscopic analysis of the oxide, the interface, and the matrix was conducted by Graham, with the results shown in table IV.[14] The segregation and depletion of chromium at the interface and from the oxide were noted.

Figure 14 is a SEM photograph of a large crack that reveals three different areas: the matrix, the oxide, and a fractured area near the center of the oxide. EDAX analyses of these three areas are listed in table V. The major components in the matrix and the oxide are iron and chromium, with some depletion of chromium in the oxides as found by Graham. Aluminum is the major component in the central portion of the oxide, apparently from the presence of aluminum oxide resulting from the oxidation of liquid aluminum alloy that had penetrated the oxide crack.

Figures 15, 16, and 17 are photomicrographs of a diagonally polished surface of a platinum-coated specimen. The oxide later developed underneath the coating, and the cracks sometimes initiated and propagated from this oxide layer. Figure 18 shows transverse metallographic specimens with a platinum coating. The remaining coating, the oxide layer, and the blisters at the fractured point of the coating are noted. The SEM photograph from this specimen in figure 19 shows that the oxide layer has developed both under and over the coating. EDAX analysis for the white band in figure 20 indicated that iron was present in the platinum coating, apparently because of intermetallic diffusion between the coating and the die steel.

Figure 21 shows a low- and a high-magnification SEM photograph of the fractured surface of a crack in the corner of a platinum-coated specimen. Aluminum oxide covered the crack opening and the surface area of the fractured oxide, as observed in figure 21. A SEM photograph taken at the crack tip of a fractured specimen shows some of the oxide and the brittle fracture of the oxide. Similar behavior was noted at the corner of the control specimen illustrated in figure 22.

Similar photographs were taken by optical microscopy in the diagonal specimens of a thermal fatigue specimen coated with molybdenum. The cracks in these specimens were filled with oxide, and in some cases the molybdenum had apparently been oxidized entirely. Oxide occurred both under and over the molybdenum coating as in the case of the platinum-coated specimen. EDAX analysis showed that the oxide layer in figure 23 had a considerably lower molybdenum content than the oxide layer in figures 24 and 25, where a bright molybdenum metal band still exists as shown by the data in table V.

Transverse and diagonal views of a tungsten-coated corner from the thermal fatigue specimen are shown in figure 26. No oxide layer was observed underneath the coating, and the crack initiated and propagated from the fractured area of the coating.

A series of photomicrographs are shown in figure 27 as the oxide layer was gradually step ground from the surface of a platinum-coated corner. Many microcracks were noted after removal of some of the lubricant-oxide layers that were perpendicular to both the long axis of the corner and the primary stress on this corner. These shallow cracks are generally not recorded during measurements of thermal crack behavior on this specimen because the removal procedure grinds them off completely. A similar series of photomicrographs, figure 28, were taken of a corner of a control specimen, and this examination indicated fewer microcracks than were present in the platinum-coated corner. The crack patterns of the platinum-coated corner and the control corner are compared in figure 29.

Crack Initiation

The appearance of oxides in all the cracks and the presence of corrosion pits in areas back from the highly stressed corner of the specimen (fig. 27) show that oxidation or corrosion is exerting an important role in crack initiation. It appears from the metallographic examination of the specimen surface that most cracks are initiated from the oxide layers in the control specimen and the molybdenum- and platinum-coated specimens. In the tungsten-coated specimen no oxidation occurred underneath the coating, but cracks did form at locations where the tungsten coating was fractured and oxidation of the H-13 die steel could occur. Crack initiation occurs preferentially at surface flaws such as pits and nicks that can be favored by corrosion and then act as stress raisers. The environment is aggressive in die casting, and the die steel is developed to exert good thermal strength rather than to resist corrosion. These circumstances plus the metallographic appearance indicate that corrosion is probably the major reason for crack initiation. Although corrosion can occur prior to the cyclic stressing effect, it is apparent that cracking is enhanced by the cyclic thermal stresses. Because of this stress the cracks propagate in the plane perpendicular to the uniaxial stress in the specimen.

The role of oxygen in initiating and propagating fatigue cracks and thermal fatigue cracks has been established in other areas. Howes[34] reports that oxidation can affect both crack initiation and propagation. Gell and Leverant[35] note that fatigue cracks can readily form within the oxide at an oxide-metal interface. Oxidation may also control the rate of fatigue crack formation because the oxide-forming materials are depleted ahead of the crack and change the composition, structure, and properties of the metal at the crack tip, making it more prone to cracking in fatigue. Other workers[36,37] have noted the role of oxygen in causing the initiation and accelerated propagation of fatigue cracks. In fact, coatings are employed in some of these cases[36] to prevent oxide formation at the surface. The microprobe analysis of the oxide area shows the depletion of chromium. This loss of chromium from the alloy plus the interaction of oxygen with the carbides[34-36] weakens the H-13 steel ahead of the corrosion pit and thus enhances thermal fatigue crack initiation and propagation ahead of the oxide-filled crack. The role of the platinum, molybdenum, and tungsten coatings, which improve the thermal fatigue resistance, is then essentially one of protecting the H-13 steel from this oxidation for as long as they remain effective. These coatings serve primarily to hinder crack initiation by preventing the formation of surface oxidation pits. Both tungsten and molybdenum do have some oxidation resistance at higher temperatures. It is reported[38] that tungsten is

effective to 600° F in lowering oxidation, and molybdenum to 400° F. Once the coating has been breeched, as shown in the photographs, the oxidation at the crack proceeds, and in some cases the strain and stress may be concentarated at fewer locations, thereby enhancing propagation.

Role of Stress

The role of stress in forming, and particularly in propagating, the crack is also apparent. The cracks propagate at right angles to the long axis of the corner or in the direction of the axial stress. The wedging action of the oxide occupying a larger volume than the metal it replaces may well add to the stress level propagating the crack by producing tensile stresses at the crack tip. It is apparent in this work that the use of large amounts of lubricant chills the surface, increases the tendency to produce tensile stresses, and increases the amount of thermal fatigue damage.

The thermal stresses produced during thermal fatigue result from the temperature differential ΔT experienced by the die surface. Since some type of upsetting is usually required for thermal fatigue cracking, the use of high-yield-strength metals and those capable of considerable plastic deformation generally reduces thermal fatigue damage. Increased thermal conductivity in the die material will result in a lower ΔT and will thus lower the stress and strain. The role of a coating material in this respect is not clear. Although it is evident that higher thermal conductivity is desirable in the base steel to reduce thermal fatigue damage, it is not clear whether the thermal fatigue resistance would be improved by having an insulator or a conductor at the surface. In any event it has been shown[29,39] that both molybdenum and tungsten have higher thermal conductivity and ductility than H-13 die steel. The yield strength of tungsten around the maximum transient temperature on the die surface (1100° F) is higher than that of H-13 steel; and the yield strength of molybdenum is about the same as that of H-13 steel at that temperature. Molybdenum and tungsten have superior strength and ductility and for these reasons may contribute to thermal fatigue resistance when they are coated on die steel.

The coatings and substrate will in general have different coefficients of thermal expansion.[2] Significant thermal expansion mismatch[40] can develop stresses and strains in a coating during thermal cycling. This tensile or compressive thermal expansion mismatch can increase or decrease the magnitude of stress and strain of the coating depending on the thermal expansion properties and thickness of the coating. It is postulated[41] that the magnitude of elastic thermal expansion mismatch between the coating and substrate might alter the strain intensity factor range ΔK_ϵ of the thermal fatigue crack and thus provide an additional driving force for fatigue crack propagation. Both molybdenum and tungsten have lower thermal expansion coefficients than H-13 die steel.[39] This thermal expansion mismatch tends to produce a tensile stress on the molybdenum and tungsten coatings. However, its net effect will depend on all the properties and test conditions.

The cyclic stresses along the edges of a thermal fatigue specimen were produced by the restrained expansion of the surface layer when the surface was heated to high temperature and the subsurface material was at low temperature. For a flat surface the stress and strain along the edge of the specimen simply depend on the temperature gradient ΔT and thermal expansion mismatch $\Delta\alpha$. When a discontinuity such as corrosion pits or

scratches forms on the surface, a stress concentration occurs at this point and this contributes to crack initiation and crack propagation. Tensile stress increases by a factor of 3.5 at the bottom of a relatively moderate scratch, as analyzed by Graham.[14] With a severe temperature cycle a large number of cracks may be initiated, and each crack can relieve the thermal strains for some distance around it. As the cracks lengthen, they begin to reduce the rate of growth of their neighbors. Under this condition some cracks eventually become dormant and other dominant. It was also found[42] that multiple notches had less effect than a single notch when the spacing between notches was less than the critical separation. The multiple-notch effect was also observed by Durelli et al.[43] with photoelastic work on the stress concentration in flat tensile test pieces.

Many thin and shallow cracks were found on the surface of the platinum-coated corner as the oxide layer was ground off the surface. These microcracks on the surface can destroy the corrosion resistance of the platinum coating, but they may alleviate the stress concentration factor. This may be a reason why the platinum-coated specimen exhibited a good thermal fatigue resistance. The crack pattern of the molybdenum-coated corner is similar to that of the control corner and does not affect the stress concentration pattern. The tungsten-coated corner accentuates the stress concentration effect because of the reduced number of cracks on the corner. However, their good corrosion resistance or superior physical properties make these coatings last for a longer period before the cracks are initiated.

CONCLUSIONS

The results of this investigation indicate that ion-deposited coatings of molybdenum, platinum, and tungsten will improve thermal fatigue resistance. Other types of coatings including silver, gold, cobalt, chromium, nickel, silver plus copper, molybdenum plus platinum, tungsten plus platinum, aluminum nitride, chromium carbide, tantalum silicate, and zirconia did not affect the thermal fatigue resistance to any significant degree. Two ion-deposited coatings, Ta_5Si_3 and silver, lowered the thermal fatigue properties.

Metallographic examinations indicated that corrosion exerted an important role in crack initiation. Coatings of molybdenum, tungsten, and platinum have better corrosion resistance to prevent the oxidation on the surface of die steel, and tungsten and molybdenum also have a high yield strength and ductility, which allows them to last longer and to protect the die steel. The alleviation of the stress concentration factor on the die surface will contribute to reducing the thermal fatigue damage. The shallow microcracks on a platinum coating appeared to reduce the stess concentration factor and to improve its thermal fatigue resistance.

REFERENCES

1. Stern, Marc: Die Casting Practice. McGraw-Hill Book Co., Inc., 1930, pp. 22-23.
2. Die Casting for Engineers. The New Jersey Zinc Co., 1946, pp. 1-5.
3. Barton, H. K.: The Pressure Diecasting of Metals. Metall. Rev., vol. 9, no. 36, 1964, pp. 305-414.
4. Street, A. C.: Developments in Pressure Diecasting. Int. Metall. Rev., vol. 20, Sept. 1975, pp. 121-136.

5. Barton, H. K.: Diecasting - Past, Present and Future, II. Eng. Digest, vol. 35, no. 10, Oct. 1974, pp. 49-55.
6. Bertolo, R. B.: Fracture Toughness of Aluminum Die Casting Die Steels. Ph.D. Thesis, Case Western Reserve University, 1976.
7. Das, S. K.: Effect of Heat Treatment on the Thermal Fatigue Behavior and Fracture Toughness of H-13 Steel for Aluminum Die Casting Dies. Ph.D. Thesis, Case Western Reserve University, 1980.
8. Comley, A. W. F.: Tool Steels for Die-Casting. Met. Ind., vol. 100, no. 8, Feb. 1962, pp. 142-146.
9. Smith, D. G.: A New Approach to an Old Problem - Die Erosion. Transactions of the Society of Die Casting Engineers, 3rd National Die Casting Congress, Paper No. 25, 1964.
10. Uddeholm Informs About Steels for Die Casting Dies. Information Bulletin, Uddenholm Steel Corporation, Stockholm, Sweden.
11. Dieter, G. E.: Mechanical Metallurgy. Second ed., McGraw-Hill Book Co., Inc., 1976, p. 449.
12. Ellison, E. G.: A Review of the Interaction of Creep and Fatigue. J. Mech. Eng. Sci., vol. 11, 1969, pp. 318-339.
13. Northcott, L.; and Baron, H. G.: The Craze-Cracking of Metals. J. Iron Steel Inst. (London), vol. 184, pt. 4, Dec. 1956, pp. 385-408.
14. Graham, R. R.: Thermal Fatigue Mechanisms in Aluminum Die Casting Die Steels. Ph.D. Thesis, Case Western Reserve University, 1978.
15. Sharp, H. J.: Aluminum Pressure Die Casting Dies - Their Failure by Surface Cracking. Met. Ind., 1953, vol. 82, no. 8, 9, and 10, 1953, pp. 141-143, 164-166, and 181-184.
16. Bengtsson, K. I.: Steels for Pressure Die Casting Dies. Met. Treat. Drop Forg., vol. 24, no. 141, June 1957, pp. 227-236.
17. Barton, H. K.: Heat Checking in Die Casting Dies. Machinery (London), vol. 91, no. 2345, Oct. 1957, pp. 982-990.
18. Brown, W. R.: A New Concept of Heat-Checking on Brass Pressure-Casting Dies. Met. Prog., vol. 63, no. 6, June 1953, pp. 73-78.
19. Fontana, M. G.; and Greene, N. D.: Corrosion Engineering. McGraw-Hill Book Co., Inc., 1967, p. 107.
20. Foroulis, Z. A., ed.: Environment-Sensitive Fracture of Engineering Materials, Proceedings of a Symposium of the Metallurgical Society of AIME Fall Meeting, 1977, Metallurgical Society, American Institute of Mining, Metallurgical and Petroleum Engineers, 1979.
21. Boyer, H. E., ed.: Metals Handbook, Vol. 10, Failure Analysis and Prevention. Eighth ed. American Society for Metals, 1975, p. 240.
22. Boyer, H. E., ed.: Metals Handbook, Vol. 10, Failure Analysis and Prevention. Eighth ed. American Society for Metals, 1975, p. 74.
23. Roberts, G. A.; and Grobe, A. H.: Service Failures of Aluminum Die-Casting Dies. Met. Prog., vol. 69, no. 2, Feb. 1956, pp. 58-61.
24. Hamaker, J. C.; and Roberts, G. A.: An Appraisal of Steels for Aluminum Die Casting Dies. Die Cast. Eng., June 1958, pp. 11-13.
25. Seth, B. B.: A Review of Heat Checking in Die Casting Dies. Die Cast. Eng., vol. 16, no. 1, Jan.-Feb. 1972, pp. 12-21.
26. Hudson, W. R.; Robson, R. R.; and Sovey, J. S.: Ion Beam Technology and Applications. NASA TM X-3517, 1977.
27. Mirtich, M. J.: Adherence of Ion Beam Sputter Deposited Metal Films on H-13 Steel. NASA TM-81585, 1980.
28. Graham, R. R.: Thermal Processing, Structure and Thermal Fatigue Relations for Die Steel. M.S. Thesis, Case Western Reserve University, 1974.

29. Benedyk, J. C.; Moracz, D. J.; and Wallace, J. F.: Thermal Fatigue Behavior of Die Materials for Aluminum Die Casting. Society of Die Casting Engineers Sixth International Die Casting Symposium and Congress, Society of Die Casting Engineers, 1970, SDCE Paper No. 111.
30. Benedyk, J. C.: Thermal Fatigue Behavior of H-13 Die Steels. Ph.D. Thesis, Case Western Reserve University, Jan. 1969.
31. Black, R. D.: Die Casting Lubricants, Their Purpose and Use. Precis. Met. Molding, vol. 16, no. 4, Apr. 1958, pp. 37-39.
32. Morris, J. R.: Lubricants as the Key to Quality Die-Casting. Allumino, vol. 43, no. 11/12, Nov.-Dec. 1974, pp. 601-608.
33. Schlomach, E.: The Effect of Spraying Duration, Lubricant Concentration, and Tool Temperature on the Lubricating Accion of Die Lubricants. Werkstatt, Bertr., vol. 107, no. 3, Mar. 1974, pp. 145-148.
34. Howes, M. A. H.: Evaluation of Thermal Fatigue Resistance of Metals Using the Fluidized Bed Technique. Fatigue at Elevated Temperatures, A. E. Carden, A. J. McEvily, and C. H. Wells, eds., American Society for Testing and Materials, ASTM STP-520, 1973, pp. 242-254.
35. Gell, M.; and Leverant, G. R.: Mechanism of High Temperature Fatigue. Fatigue at Elevated Temperatures, A. E. Carden, A. J. McEvily, and C. H. Wells, eds., American Society for Testing and Materials, ASTM STP-520, 1973, pp. 37-67.
36. Merrick, H. F.; Maxwell, D. H.; and Gibson, R. C.: Fatigue in the Design of High Temperature Alloys. Fatigue at Elevated Temperatures, A. E. Carden, A. J. McEvily, and C. H. Wells, eds., American Society for Testing and Materials, ASTM STP-520, 1973, pp. 285-299.
37. Ellison, E. G.; and Smith, E. M.: Predicting Service Life in a Fatigue-Creep Environment. Fatigue at Elevated Temperatures, A. E. Carden, A. J. McEvily, and C. H. Wells, eds., American Society for Test- ing and Materials, ASTM STP-520, 1973, pp. 575-612.
38. Huminik, J., Jr.: High Temperature Inorganic Coatings. Reinhold Publishing Corp., 1963, pp. 281-282.
39. Noesen, S. J.; and Williams, H. A.: The Thermal Fatigue of Die Casting Dies. Mod. Cast., vol. 51, no. 6, June 1967, pp. 119-132.
40. Strangman, T. E.: Fatigue Crack Initiation and Propagation in Electron Beam Vapor Deposited Coatings for Gas Turbine Superalloys. Thin Solid Films, vol. 45, 1977, pp. 499-506.
41. Strangman, T. E.; and Hopkins, S. W.: Thermal Fatigue of Coated Superalloys. Am. Ceram. Soc. Bull., vol. 55, no. 3, Mar. 1976, pp. 304-307.
42. Baron, H. G.; and Bloomfield, B. S.: Resistance to Thermal Stress Fatigue of Some Steels, Heat-Resisting Alloys, and Cast Irons. J. Iron Steel Inst. (London), vol. 197, pt. 3, Mar. 1961, pp. 223-232.
43. Durelli, A. J.; et al.: Stress Concentrations Produced by Multiple Semi-Circular Notches in Infinite Plates Under Uniaxial State of Stress. Proceedings of the Society for Experimental Stress Analysis, Vol. 10, C. V. Mahlmann and W. M. Murray, eds., Society for Experimental Stress Analysis, 1952, pp. 53-64.

TABLE I. - COMPOSITION OF H-13 STEELS INVESTIGATED

Element	R (round bar), heat 95996-V3	S (square bar), heat 24763
	Content, percent	
C	0.39	0.44
Mn	.41	.20
Si	1.00	1.40
Ni	.32	.40
Cr	4.90	5.00
Mo	1.30	1.35
V	.90	.91
Cu	.07	.12
Al	.076	.014
S	.006	.002
P	.015	.012

TABLE II. - HEAT TREATMENT AND HARDNESS

Process	R (round bar)			S (square bar)		
	Temperature, °F	Time, hr	Hardness, R_C	Temperature, °F	Time, hr	Hardness, R_C
Austenitize	1850	2	----	1850	2	----
First temper	1100	1	53	1100	1	52
Second temper	1100	1	50.5	1100	1	49.5
Third temper	1100	3.5	46	1100	3.5	45.5

TABLE III. - THERMAL FATIGUE TEST RESULTS OF H-13 STEEL WITH VARIOUS ION-DEPOSITED COATINGS

Specimen description		Maximum crack length, d, μm	Crack area, Σnd^2, μm^2
R1	Control	23×10^2	101.7×10^6
	0.17 μm Mo/1.0 μm Pt	31	117.1
	0.17 μm W/1.0 μm Pt	33	140.6
	1.0 μm Pt	17	60.0
R2	Control	25×10^2	100.2×10^6
	Radius of corner too large		
	1.0 μm Pt	20	58.1
	1.0 μm W	24	41.5
R4	Control	25×10^2	80.4×10^6
	1.0 μm Si_3N_4	23	59.2
	1.0 μm W	31	67.4
	1.0 μm Pt	11	36.6
R5	Control	39×10^2	101.1×10^6
	1.0 μm AlN	27	100.2
	1.0 μm Cr_3C_2	28	86.1
	1.0 μm Si_3N_4	27	66.1
R7	Control	37×10^2	126.0×10^6
	0.5 μm W	38	171.0
	1.0 μm W	27	86.1
	2.0 μm W	29	74.2
S2	Control	25×10^2	65.2×10^6
	1.0 μm Ta_5Si_3	32	87.9
	1.0 μm Mo	15	29.7
	1.0 μm ZrO_2	28	47.7
R4	Control	10×10^2	15.4×10^6
	1.0 μm Co	10	62.3
	1.0 μm Au	10	58.3
	1.0 μm W	2.5	.27
R8	Control	8×10^2	13.0×10^6
	1.0 μm Mo	14	24.6
	1.0 μm Cr	16	42.2
	1.0 μm Ni	16	33.4
R9	Control	12×10^2	36.4×10^6
	1.0 μm Ag/Cu	10	20.1
	1.0 μm Pt	9	13.2
	1.0 μm Ag	16	77.0
S1	Control	11×10^2	23.1×10^6
	Control	15	10.8
	Control	18	21.7
	Radius of corner too large		

TABLE IV. - MICROPROBE READINGS IN AREA OF THERMAL FATIGUE CRACKS IN H-13 STEEL AND THERMAL FATIGUE SPECIMEN (REF. 14)

Element	Matrix	Oxide	Interface
	Relative amount of the elements present[a]		
Cr	7550	3880	12 850
S	105	73	80
N	950	-----	1 050
Si	130	-----	80
Mo	135	-----	205
V	1220	-----	3 020
Cu	750	-----	850
Al	35	----	60

[a] Readings can be converted to approximate percentages based on the following values of 100 percent for the various elements:

Element	100 Percent readings (CPS * 10)
Cr	60 000
S	42 000
Ni	135 000
Si	18 000
Mo	20 000
V	50 000
Cu	135 000
Al	14 000

TABLE V. - EDAX READINGS IN AREAS OF THERMAL FATIGUE CRACKS AND COATINGS

Description	Element	Oxide content, wt %
Matrix (fig. 14)	V Cr Fe	0.091 5.563 93.455
Oxide (fig. 14)	V Cr Fe	0.811 4.951 94.238
Crack center (fig. 14)	Al Si Ca Fe Cu Zn	43.780 5.290 20.227 13.306 6.387 11.010
Platinum coating (area selected in white band in fig. 20)	Fe Pt	26.675 73.325
Molybdenum coating (area selected in surface oxide in fig. 23)	Mo Cr Fe Zn	2.289 7.322 88.646 1.742
Molybdenum coating (area selected around surface coating in figs. 24 and 25)	Mo Fe Zn	23.161 47.685 29.154

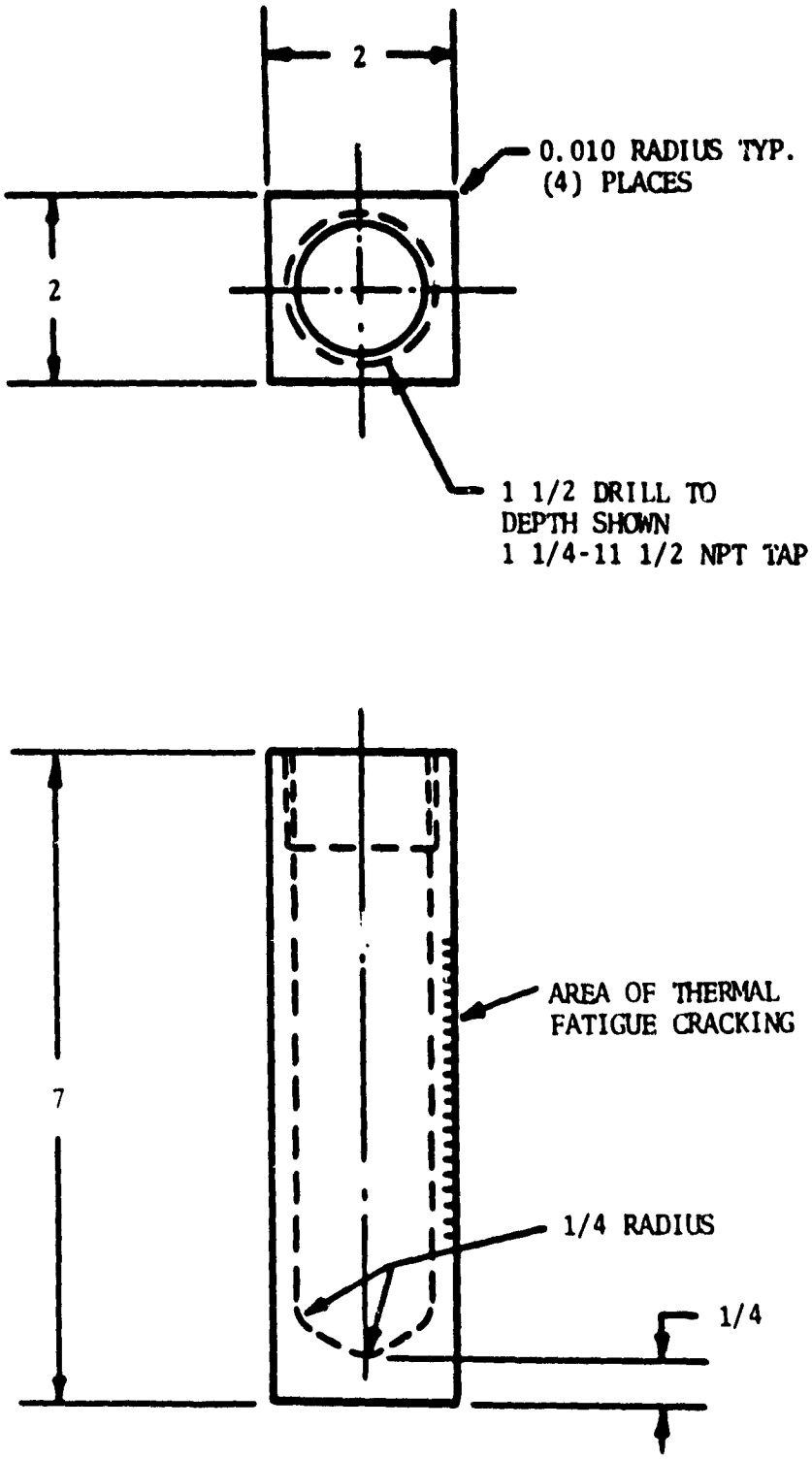

FIGURE 1: THERMAL FATIGUE SPECIMEN (1/2 SIZE)

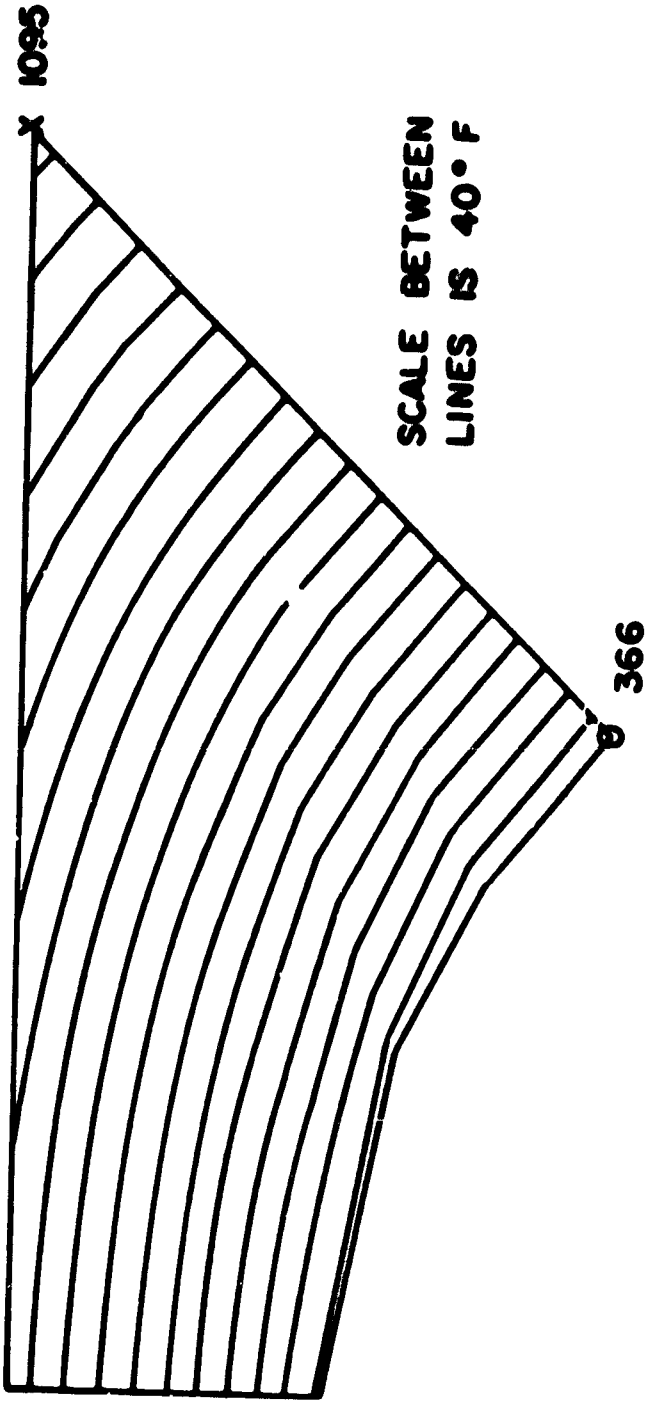

FIGURE 2: TEMPERATURE PROFILE THROUGH THERMAL FATIGUE SPECIMEN 12 SECONDS AFTER IMMERSION. (REF 14)

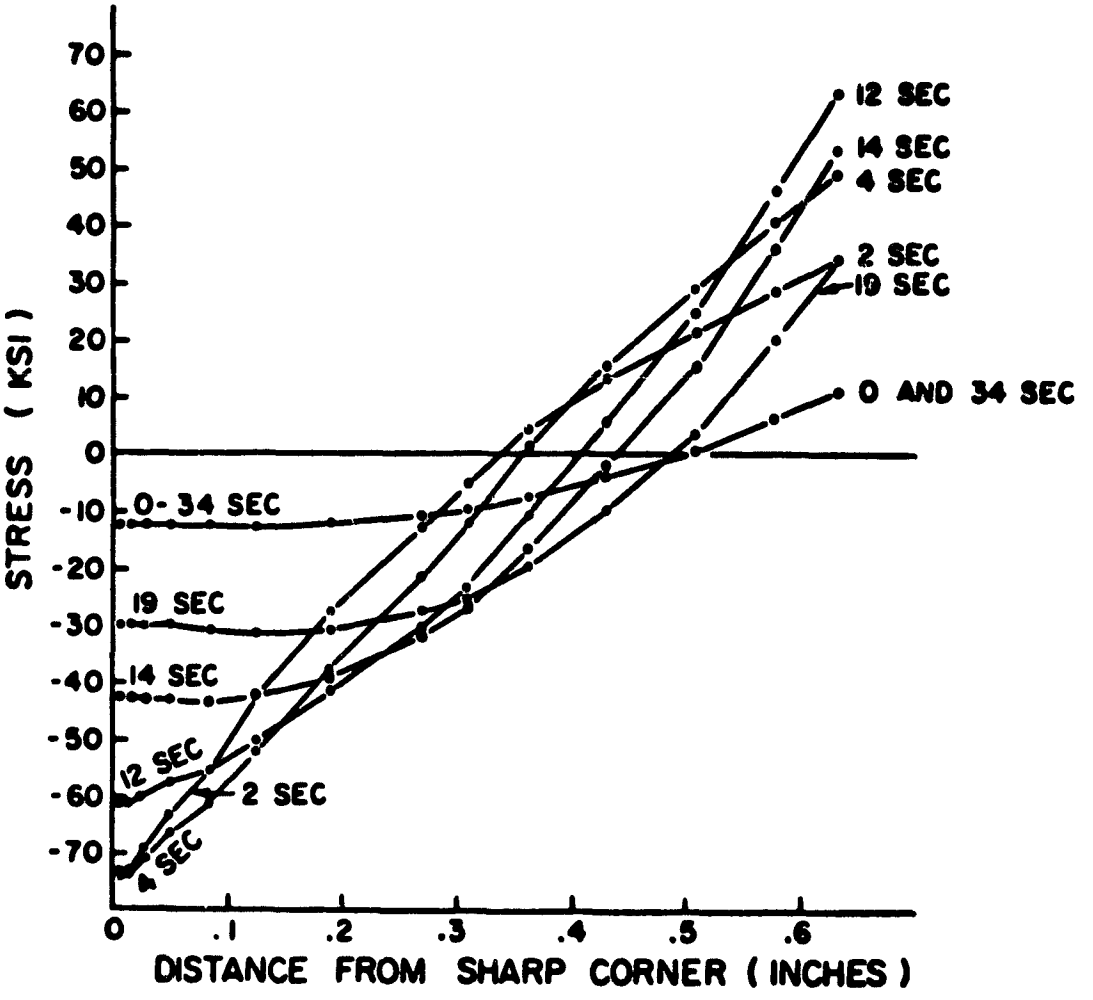

FIGURE 3: VERTICAL STRESS AT CENTROIDS OF ELEMENTS ALONG DIAGONAL CENTERLINE. (REF 14)

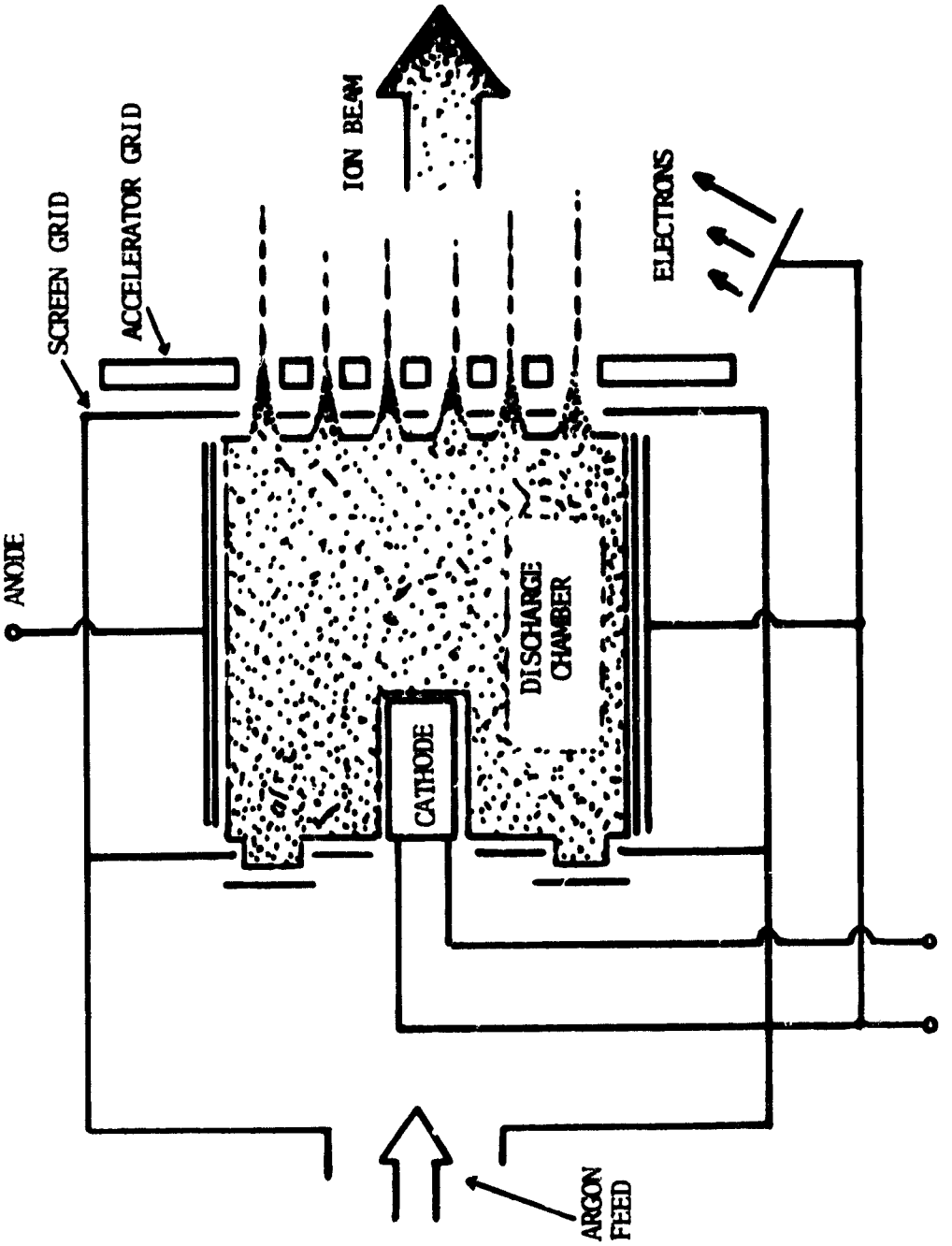

FIGURE 4: DISCHARGE CHAMBER

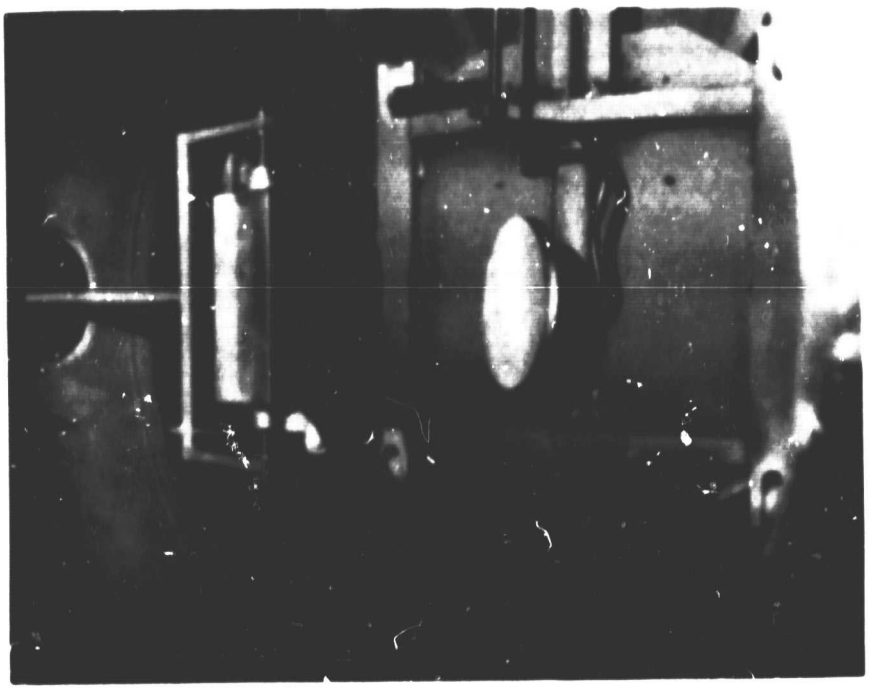

FIGURE 5: SPECIMEN POSITION DURING COATING

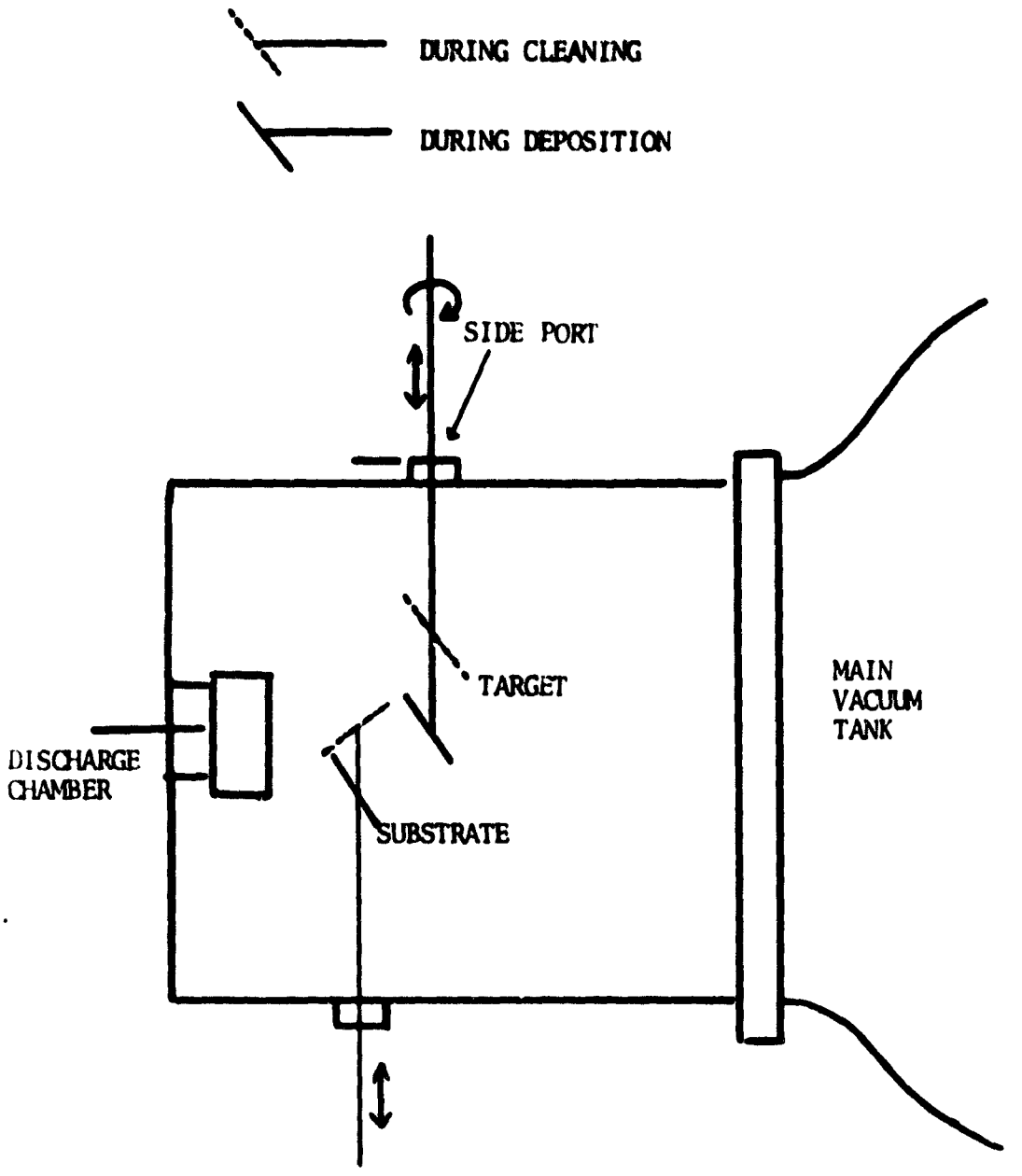

FIGURE 6: RELATIVE POSITION OF ION BEAM, TARGET, AND SUBSTRATE.

FIGURE 7: THE ACTUAL VIEW OF ION BEAM SPUTTER DEPOSITION EQUIPMENT.

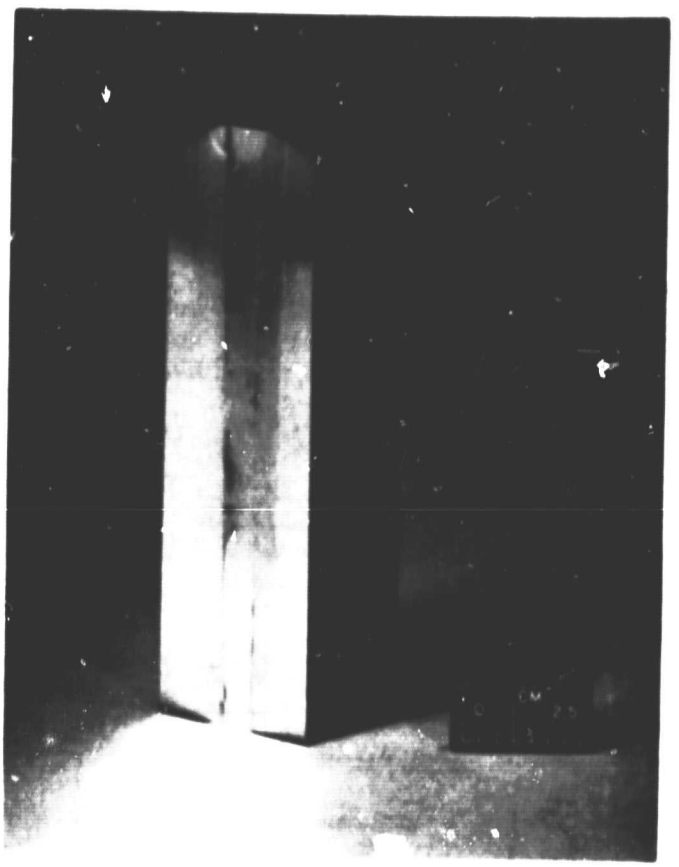

FIGURE 8: A COATED SPECIMEN, FROM LEFT TO RIGHT ARE COBALT, GOLD AND TUNGSTEN COATINGS.

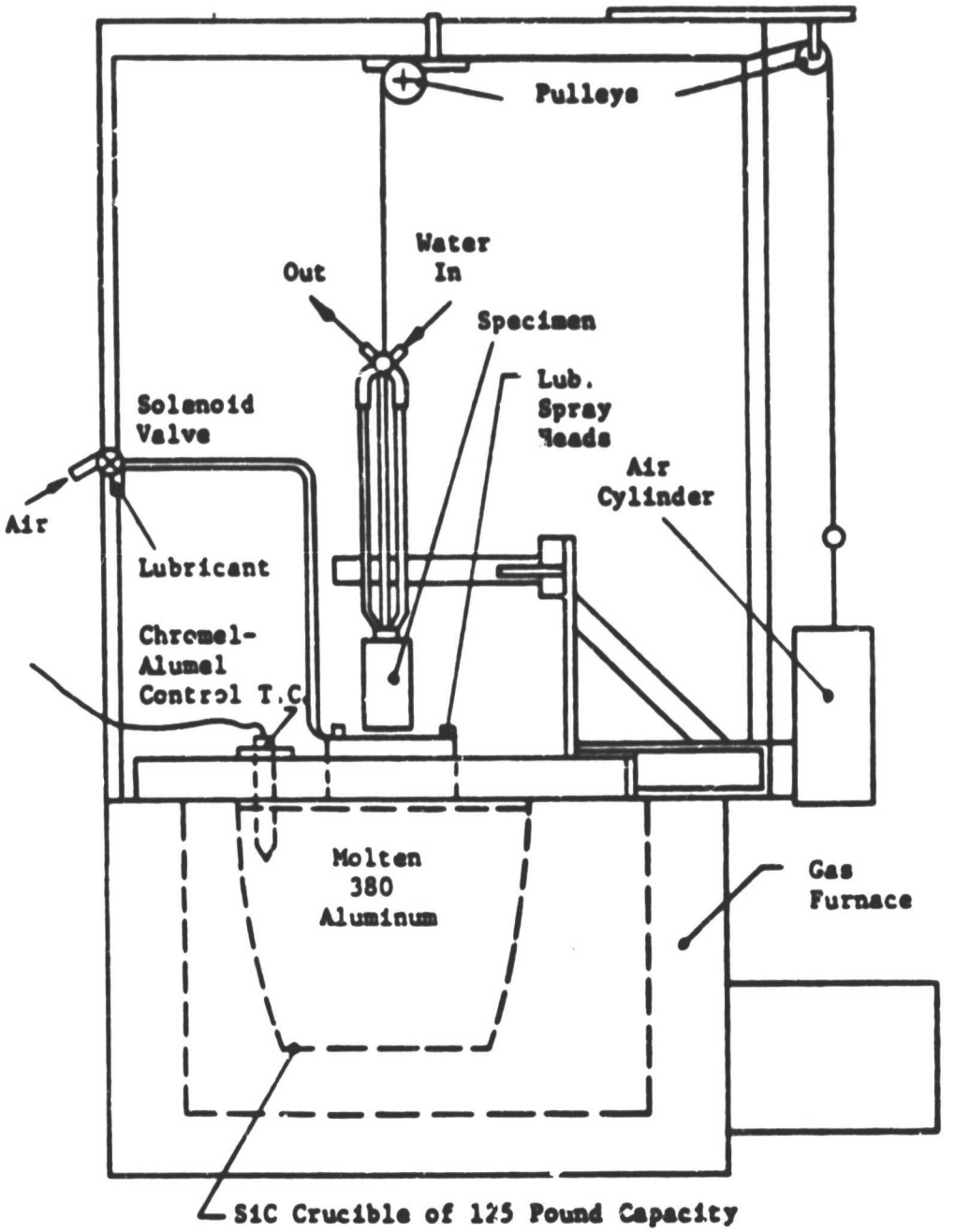

FIGURE 9: THERMAL FATIGUE TEST EQUIPMENT.

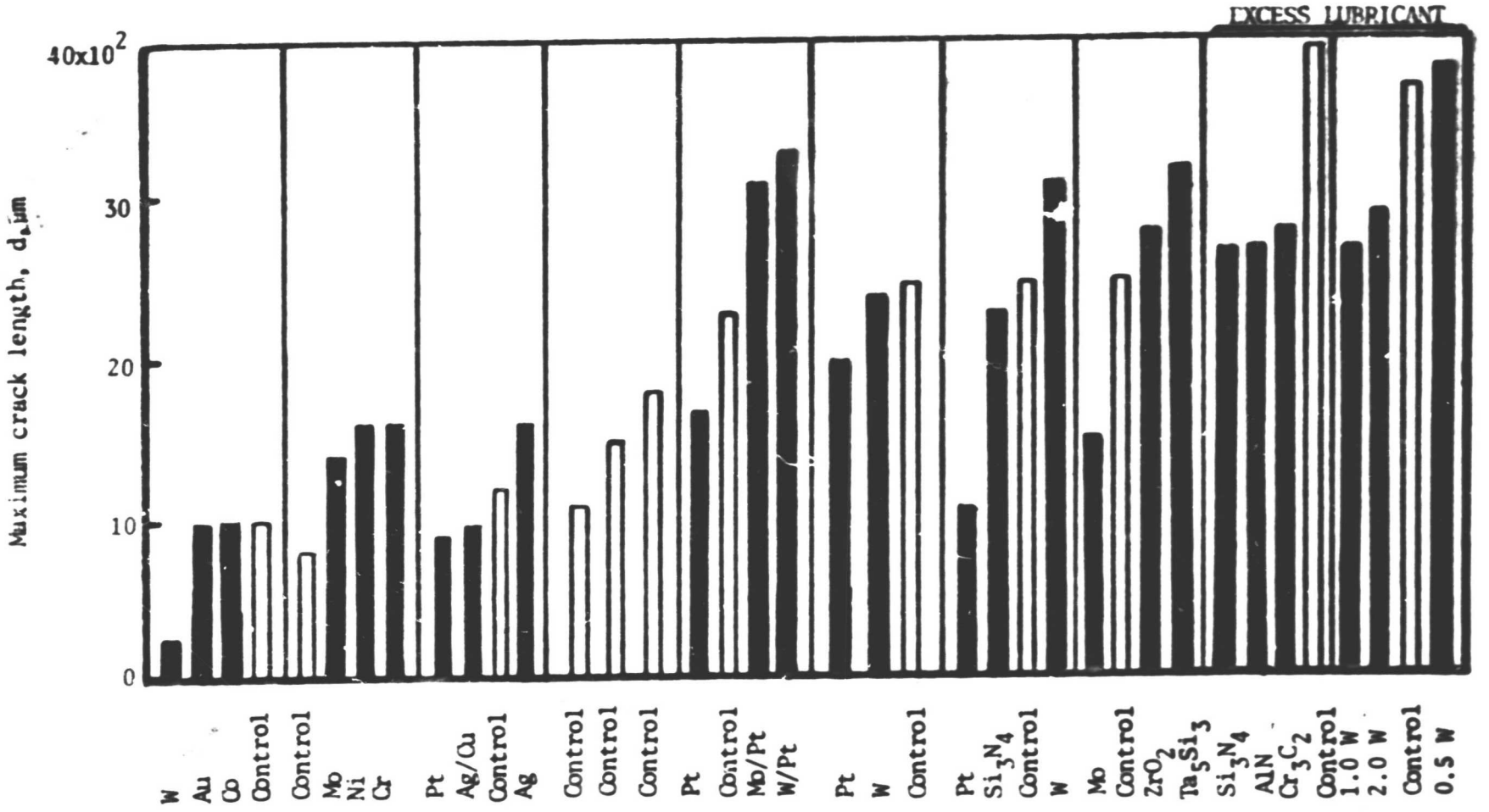

FIGURE 10: MAXIMUM CRACK LENGTH PARAMETER OF THERMAL FATIGUE BEHAVIOR OF SPECIMEN WITH VARIOUS COATINGS

FIGURE 11: CRACKED AREA PARAMETER OF THERMAL FATIGUE BEHAVIOR OF SPECIMEN WITH VARIOUS COATINGS

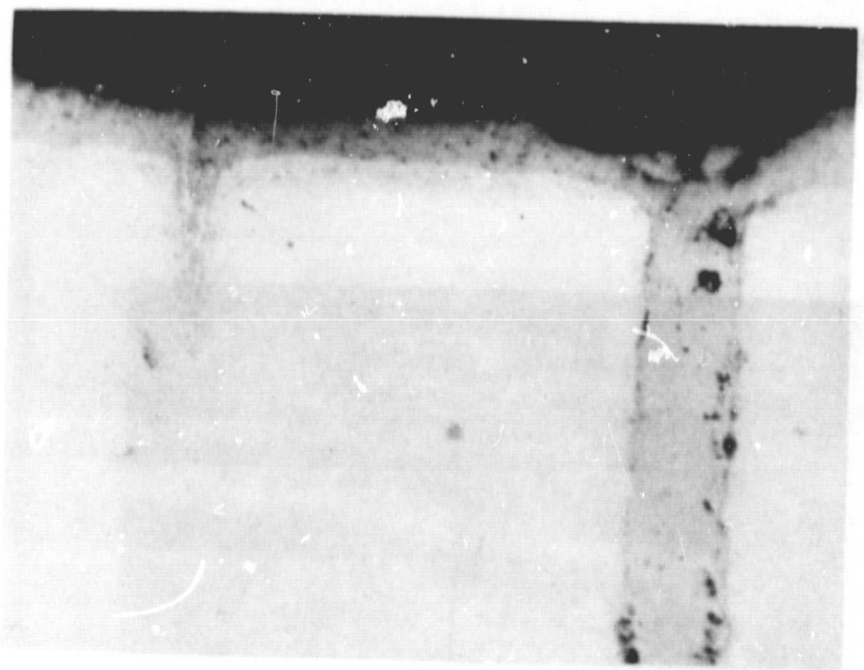

FIGURE 12: THE DIAGONAL VIEW OF CONTROL CORNER. CRACKS ARE INITIATED FROM THE OXIDE LAYER. (MAG 500X)

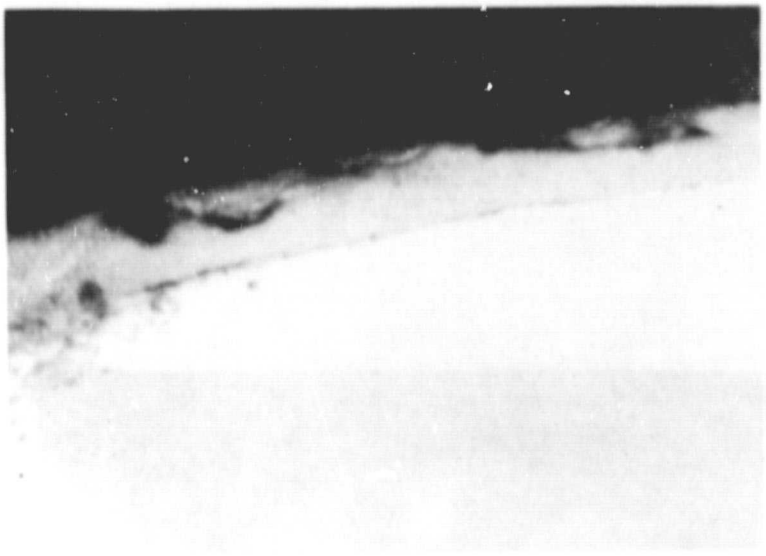

(a)

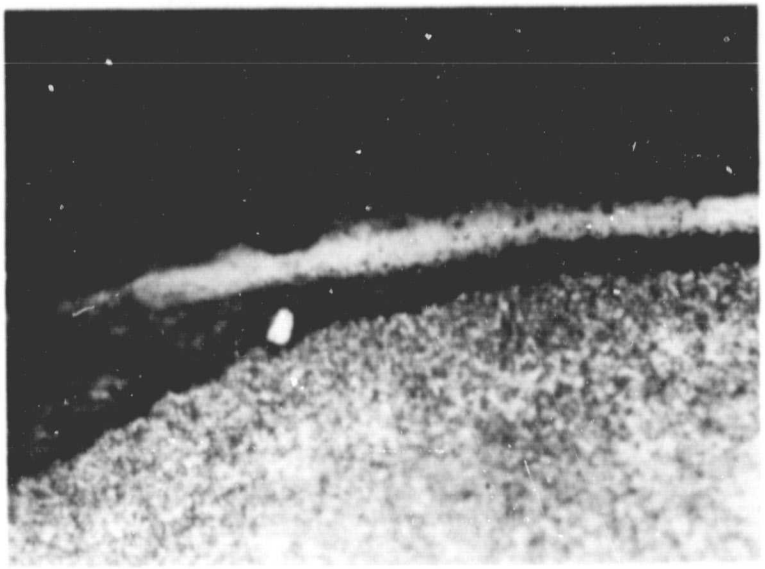

(b)

FIGURE 13: (a) THE TRANSVERSE VIEW OF THE CONTROL SPECIMEN. LIGHT GRAY AREA IS OXIDE LAYER COVERED ON THE MATRIX (WHITE AREA). (b) SAME AREA ETCHED BY 4% NITAL, NOTE THE AREA NEARBY THE OXIDE LAYER IS MORE REACTIVE TO ETCHING SOLUTION. (MAG 500X)

FIGURE 14: THE DIAGONAL VIEW OF A CRACK AROUND THE CRACK OPENING; MATRIX, OXIDE AND CRACKED CENTRAL PART FORM THREE DISTINGUISHED AREAS. (MAG 1000X)

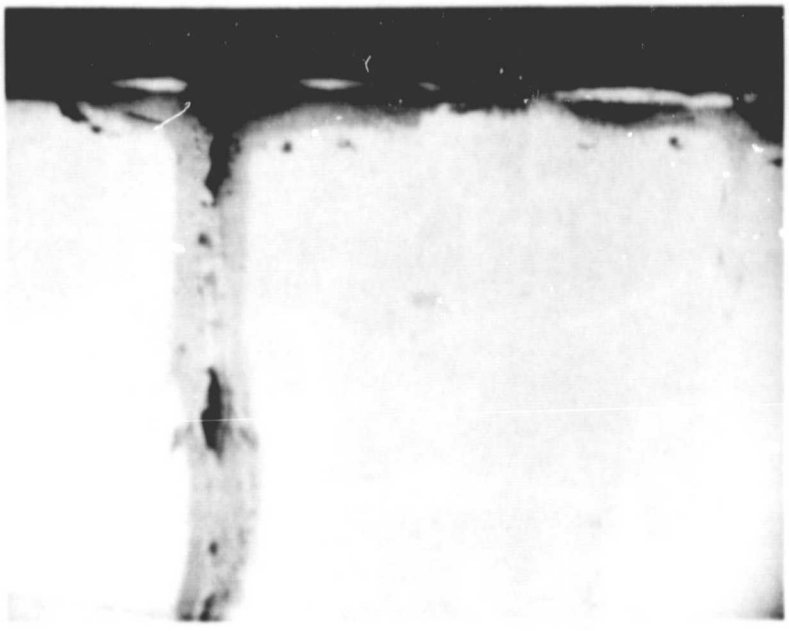

FIGURE 15: THE DIAGONAL VIEW OF PLATINUM COATED CORNER .CRACKS ARE INITIATED FROM THE OXIDE LAYER UNDERNEATH THE COATING. (MAG 500X)

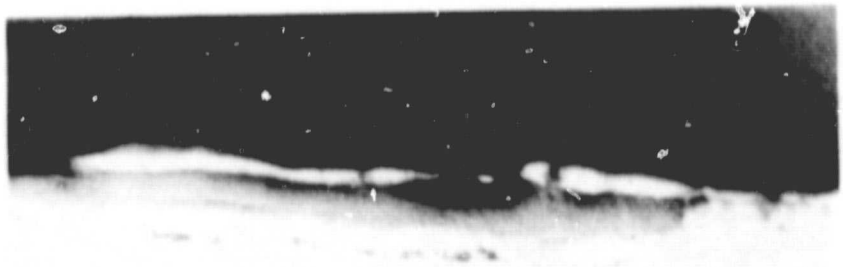

FIGURE 16: THE DIAGONAL VIEW OF PLATINUM COATED CORNER. OXIDE DEVELOPED UNDERNEATH THE COATING BUT NO CRACK FORMED YET. (MAG 500X)

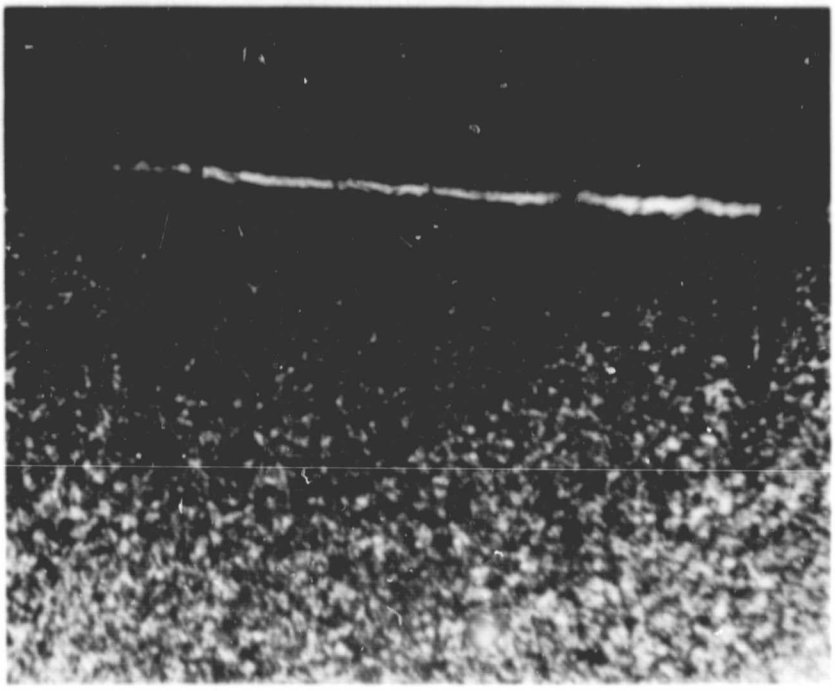

FIGURE 17: THE DIAGONAL VIEW OF PLATINUM COATED SPECIMEN. OXIDE DEVELOPED UNDERNEATH THE COATING AND SMALL CRACKS BEGIN TO CUT INTO THE MATRIX AT SOME FRACTURED POINTS OF THE COATING. (MAG 500X)

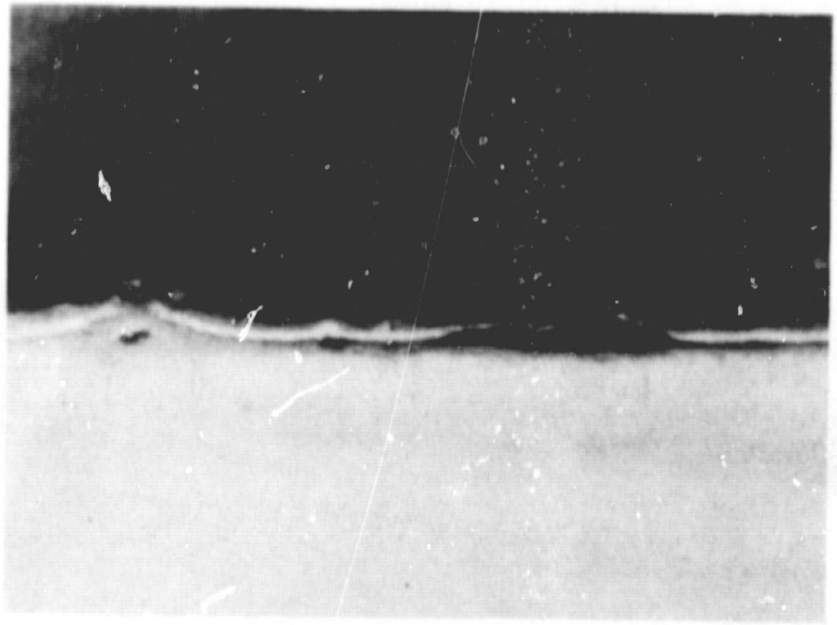

(a)

(b)

FIGURE 18: THE TRANSVERSE VIEW OF PLATINUM COATING. (a) WHITE LINE AND GRAY RIBBON IN THE CENTER OF THE PICTURE ARE COATING AND OXIDE. (b) SAME AREA ETCHED BY 4% NITAL SOLUTION. (MAG 500X)

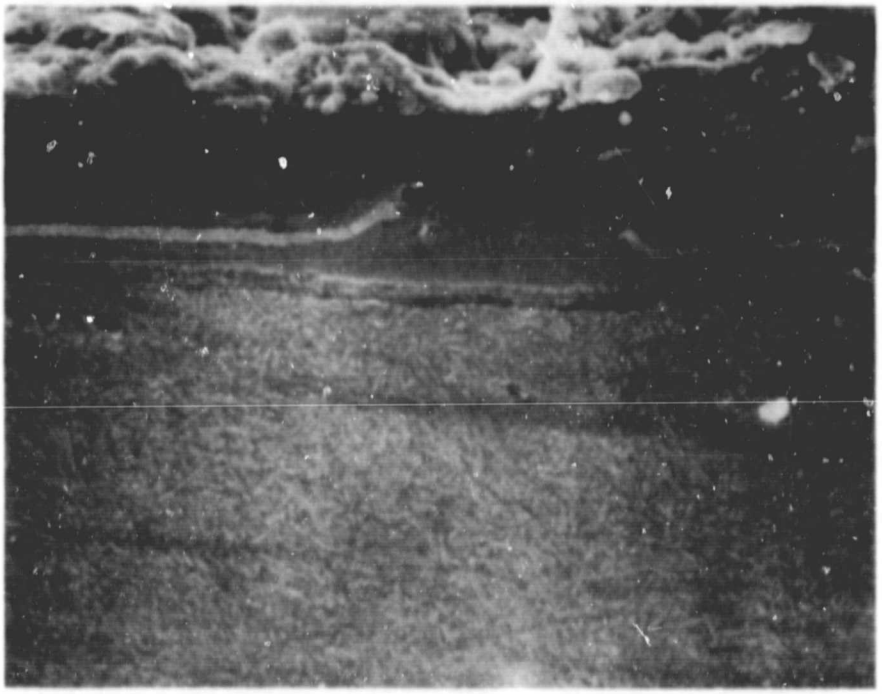

FIGURE 19: SEM MICROSCOPY OF PLATINUM COATING. FRACTURED POINT OF THE COATING AND OXIDE DEVELOPDE UNDER AND OVER THE COATING ARE OBSERVED. (MAG 500X)

FIGURE 20: AN ENLARGED VIEW OF FIGURE 19 IN AREA AROUND FRACTURED POINT. (MAG 5000X)

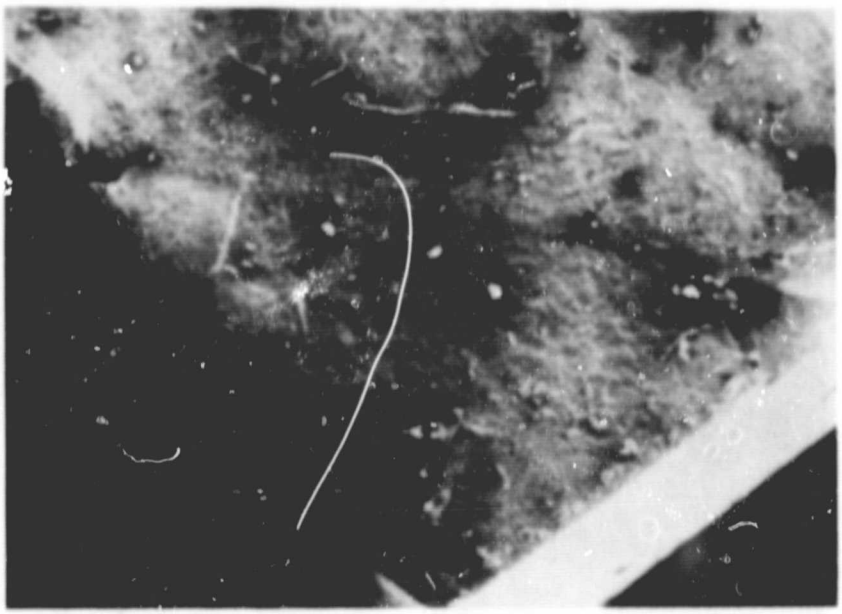

(a) MAG 20X

(b) MAG 1000X

FIGURE 21: SEM MICROSCOPY OF TRANSVERSELY FRACTURED SURFACE OF PLATINUM COATED SPECIMEN. (a) CORROSION ATTACKED AREA OF THE THERMAL FATIGUE CRACK ARE OBSERVED. (b) AN ENLARGED VIEW OF TOP PICTURE IN AREA AROUND THE CORNER, OXIDE SCALE COVERED THE FRACTURED SURFACE ARE OBSERVED.

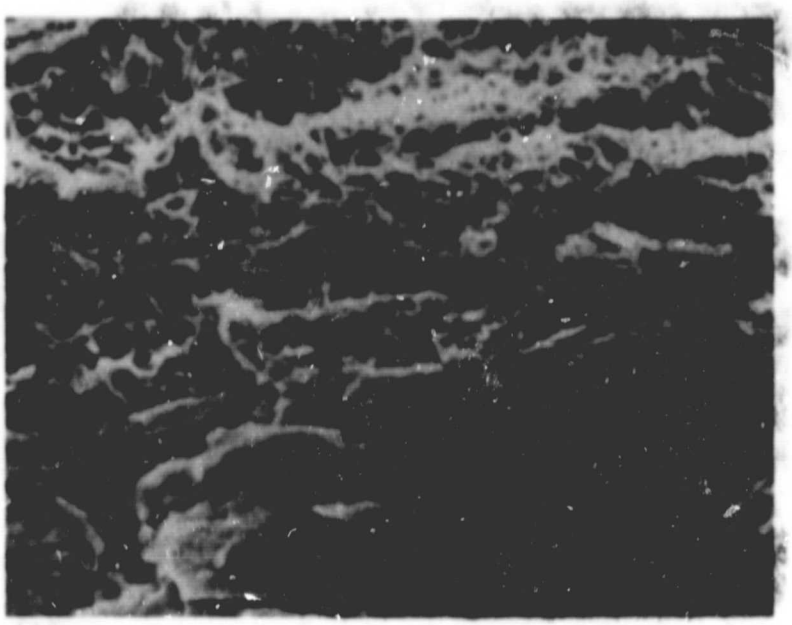

(a)

(b)

FIGURE 22: SEM MICROSCOPY OF CRACK FRONT OF CONTROL SPECIMEN. (a) THE BRITTLE CHARACTERISTICS OF OXIDIZED AREA AT LOWER PART OF THE PICTURE ARE OBSERVED. (MAG 1000X). (b) AN ENLARGED VIEW OF SAME AREA AS (a). (MAG 5000X)

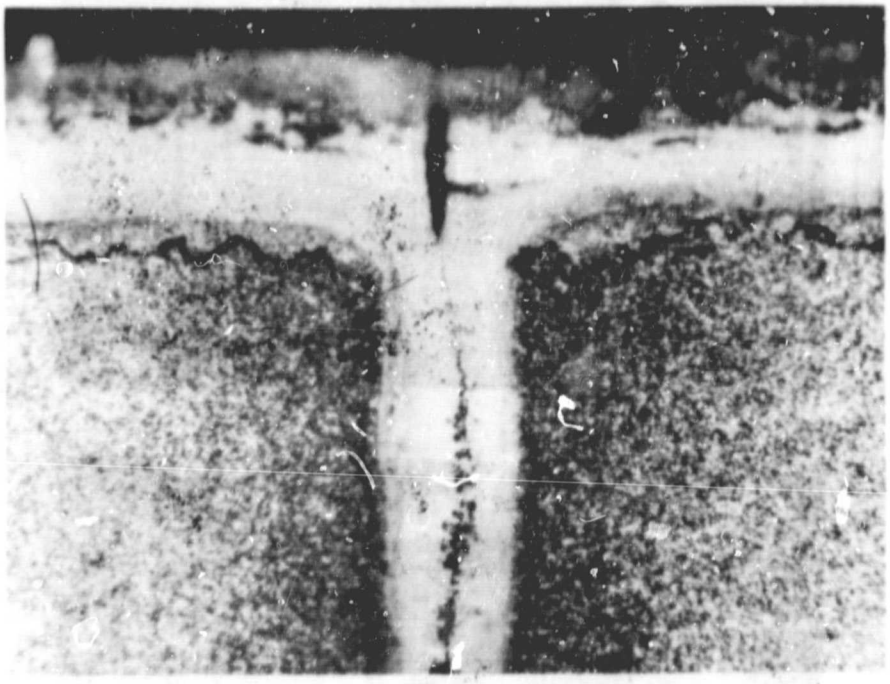

FIGURE 23: A DIAGONAL VIEW OF MOLYBDENUM COATED CORNER. THICK OXIDE LAYER AND CRACK ARE SIMILAR TO CONTROL CORNER. EDAX ANALYSIS RESULTS OF THIS OXIDE LAYER INDICATE MOST MOLYBDENUM HAD BEEN GONE, SEE TABLE V. (MAG 500X)

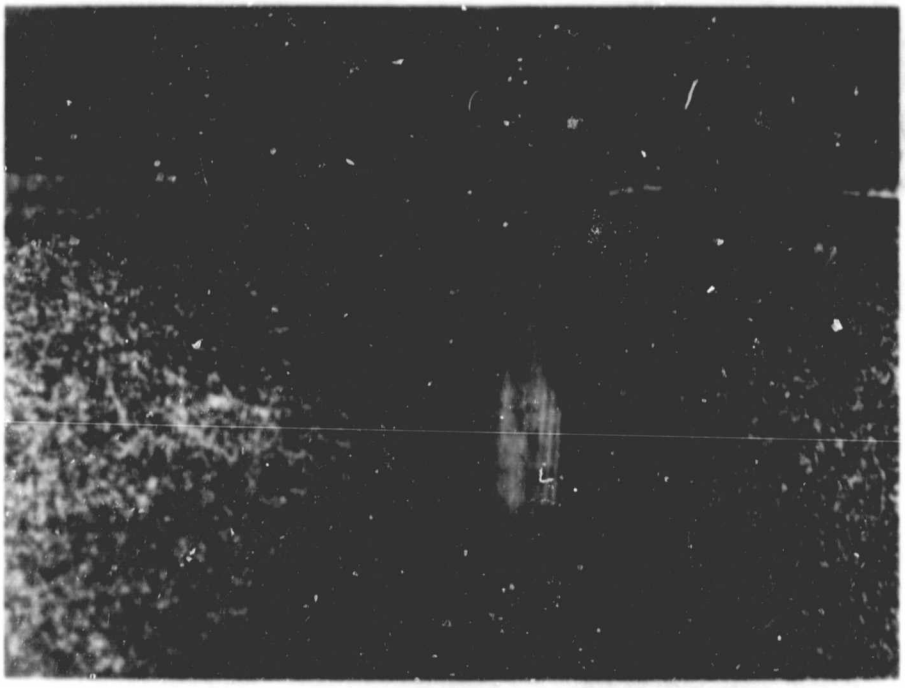

FIGURE 24: A DIAGONAL VIEW OF MOLYBDENUM COATED CORNER. THE THINNER OXIDE LAYER WITH COATING IN THE RIGHT PART OF THIS PICTURE IS OBSERVED. (MAG 500X)

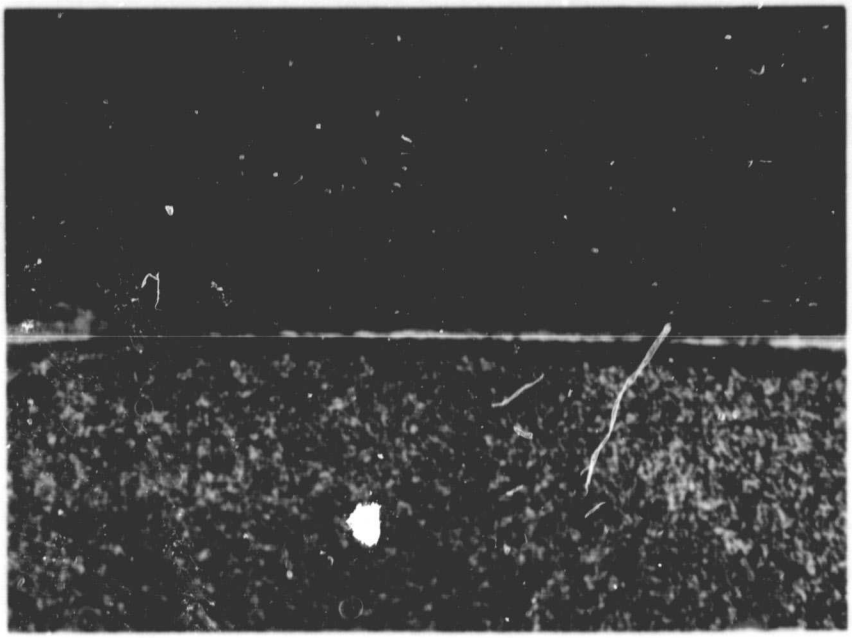

FIGURE 25: A DIAGONAL VIEW OF MOLYBDENUM COATED SPECIMEN. THE WHITE LINE IN THE CENTER OF THIS PICTURE IS THE REMAINING COATING. EDAX ANALYSIS AROUND THIS AREA INDICATES MOLYBDENUM STILL EXISTS, SEE TABLE V. (MAG 500X)

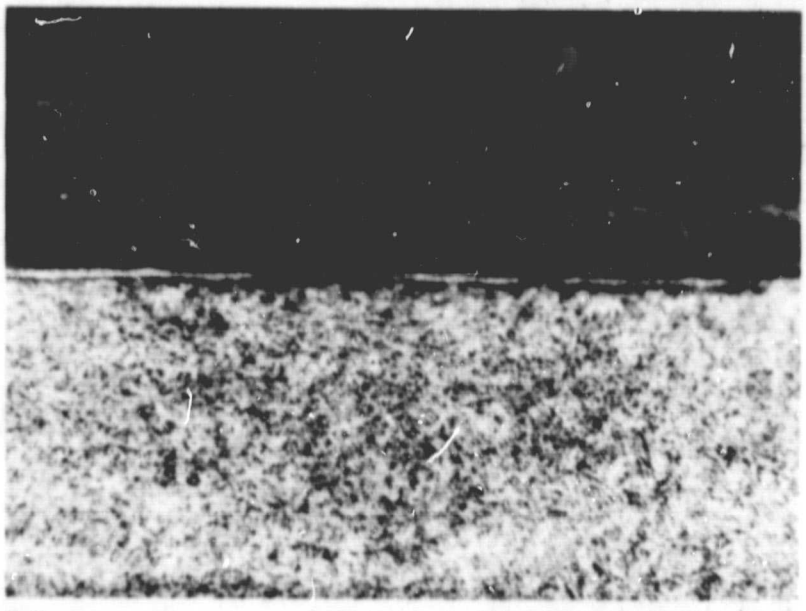

(a)

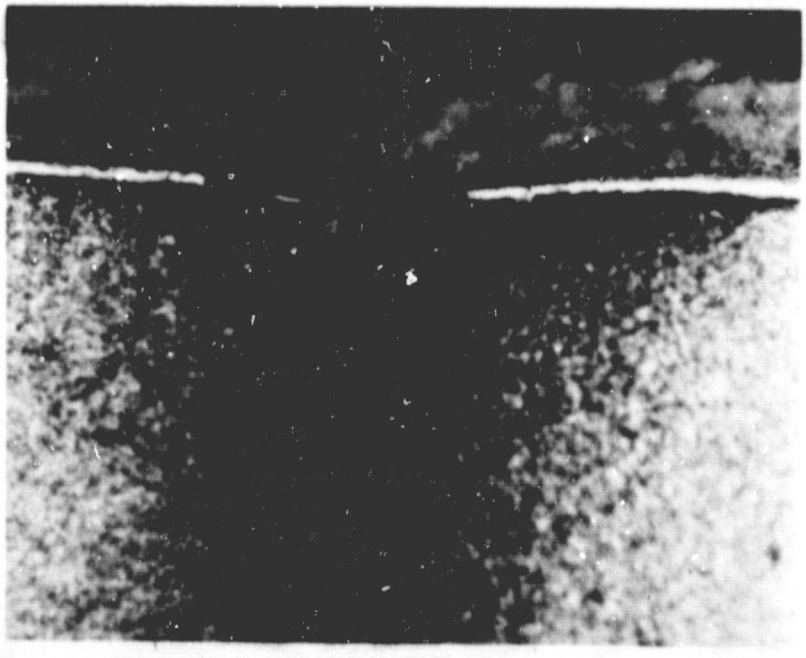

(b)

FIGURE 26: (a) THE TRANSVERSE VIEW OF TUNGSTEN COATED SPECIMEN. (b) THE DIAGONAL VIEW OF TUNGSTEN COATED SPECIMEN. IT IS NOTED THAT NO OXIDES ARE DEVELOPED UNDERNEATH THE COATING. (MAG 500X)

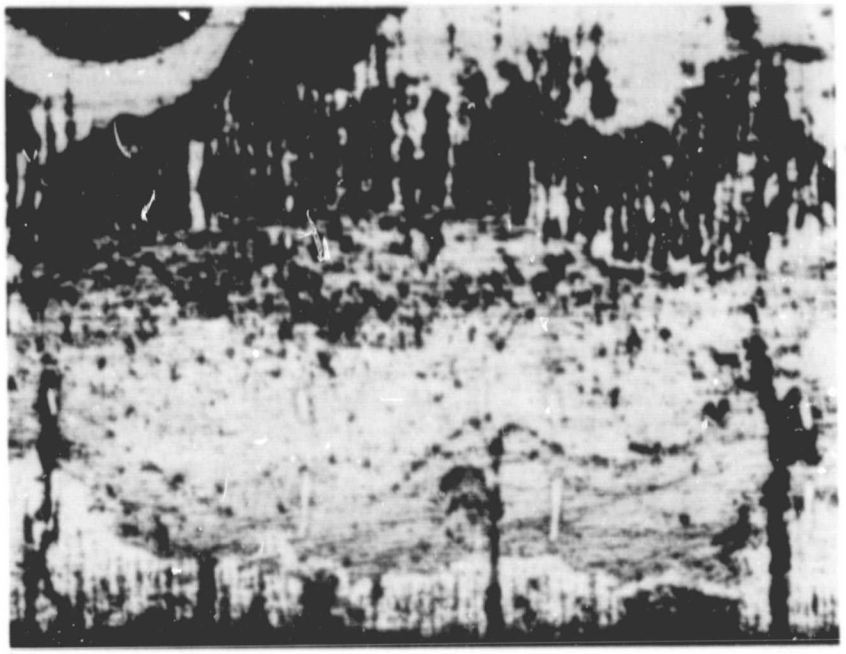

(a)

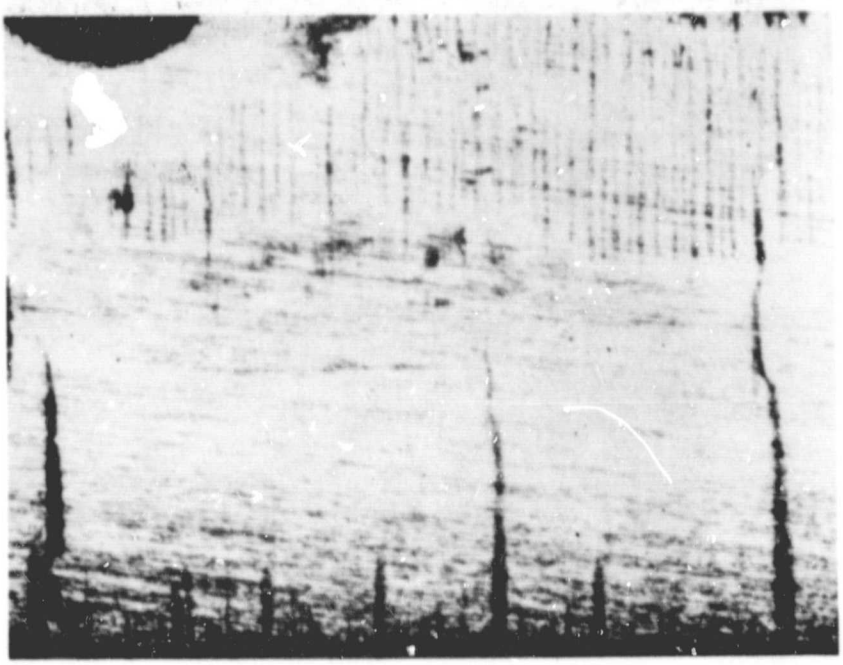

(b)

FIGURE 27: PROGRESSIVE REMOVAL OF SURFACE OXIDE LAYER OF PLATINUM COATED SPECIMEN. (a) GROUND OFF 5 μ . (b) 10 μ . (MAG 60X)

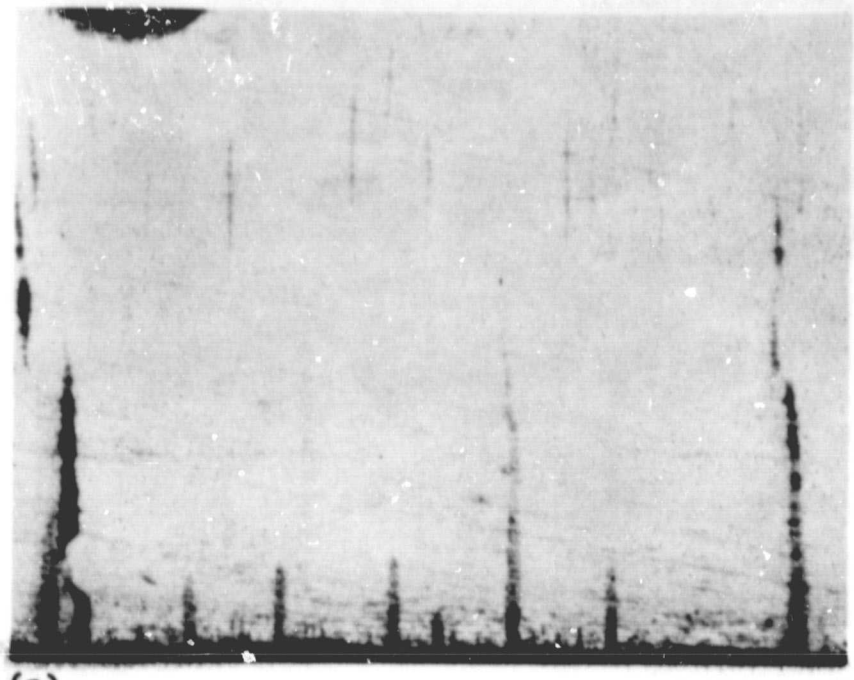

(c)

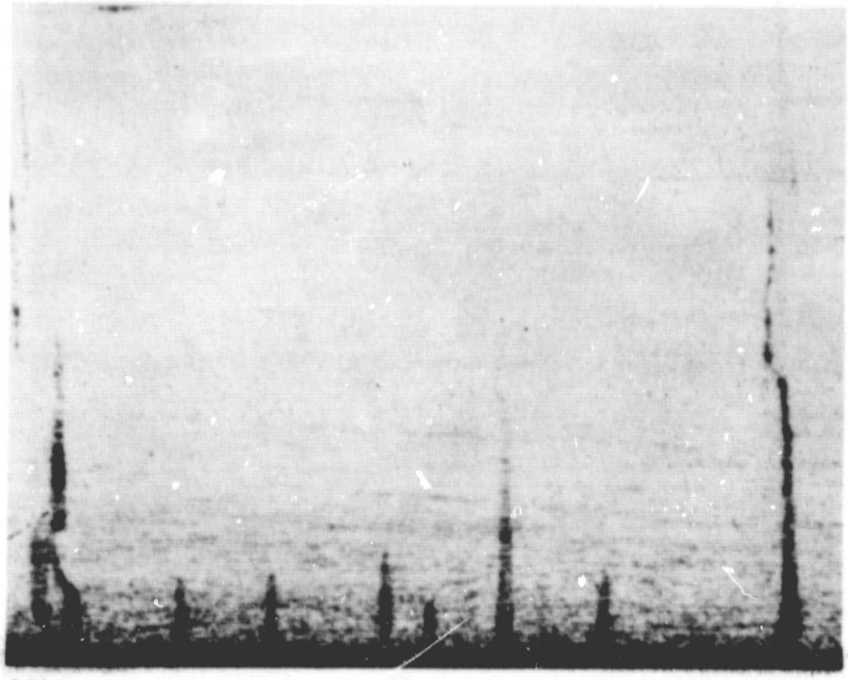

(d)

FIGURE 27: (con't). (c) 15 μ . (d) 25 μ. (MAG 60X)

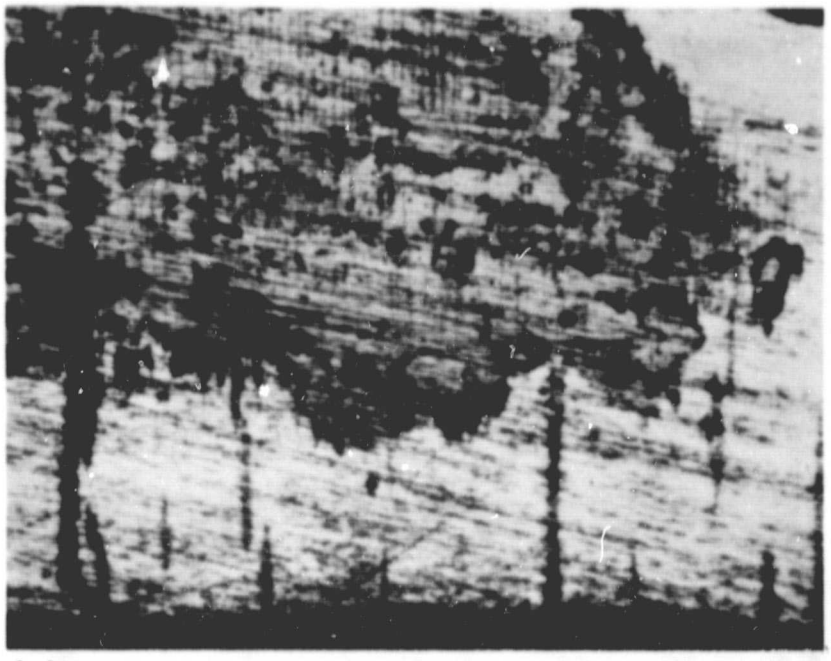

(a)

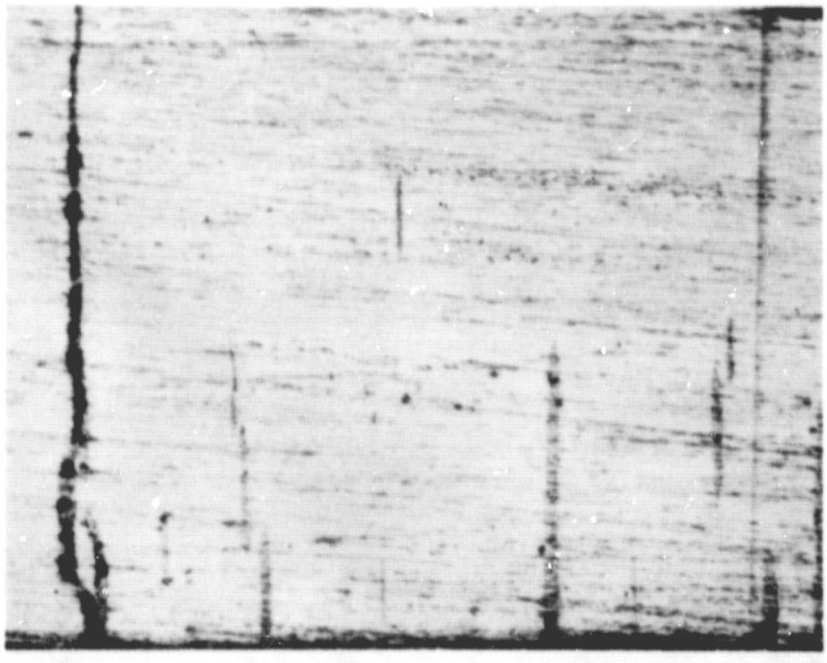

(b)

FIGURE 28: PROGRESSIVE REMOVAL OF SURFACE OXIDE LAYER OF CONTROL SPECIMEN. (a) 7 μ. (b) 15 μ. (MAG 60X)

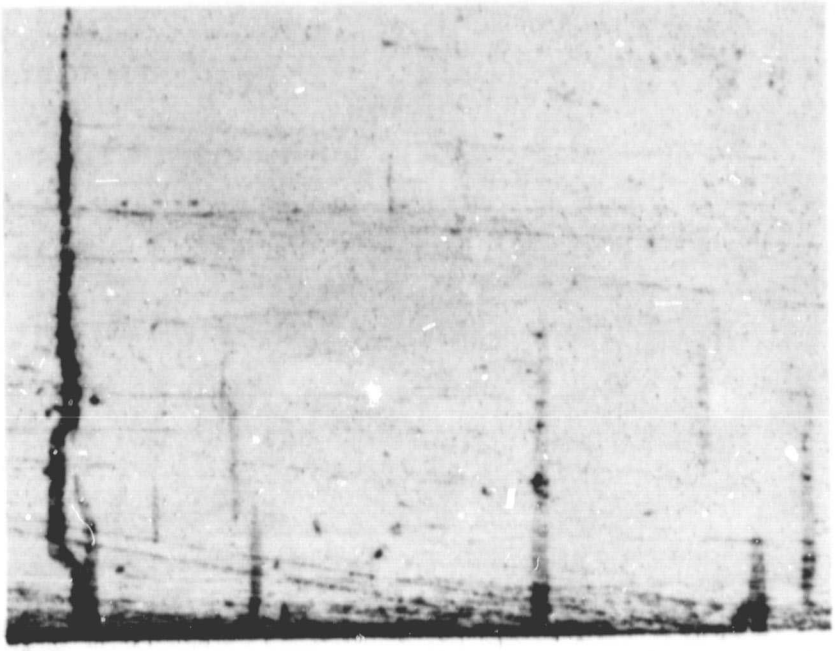

(c)

FIGURE 28: (con"t). (c) 20 μ. (MAG 60X)

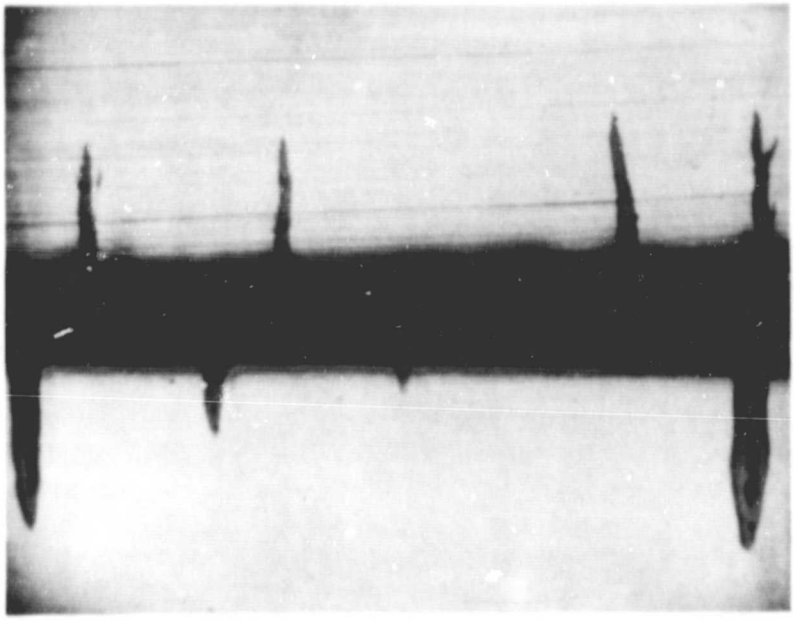

FIGURE 29: COMPARISON OF DIAGONAL VIEW OF CRACK PATTERNS BETWEEN PLATINUM COATED SPECIMEN(TOP) AND CONTROL SPECIMEN (BOTTOM). (MAG 100X)